Photochemical Synthesis of Niobium Nanoparticles

Dimitriy Malyshev

Thesis submitted to the
Faculty of Graduate and Postdoctoral Studies
in partial fulfillment of the requirements for the degree of
Master of Science
Specialization in Chemistry
in the Ottawa-Carleton Chemistry Institute
Department of Chemistry, University of Ottawa

Université d'Ottawa · University of Ottawa

Candidate

Dimitriy Malyshev

Supervisor

Professor J. C. Scaiano

To my parents,

For their boundless love and support.

Abstract

This thesis focuses on the development of method to the photochemical synthesis of niobium nanoparticles (NbNP) using Irgacure 907 (I-907) photoinitiator. This investigation is composed of two parts; whereas the mechanistic study of formation of particles was investigated first, and then followed by particles property characterization. By studying the mechanism of formation we were able to obtain knowledge on how to control the size of NbNP. This knowledge provided us with ability to generate a library of nanoparticles with the varying sizes. Furthermore, the study of I-907 photoproducts has given insight for an alternative method for the synthesis of NbNP using a milder reducing agent, 4-(methylthio)benzaldehyde (MSBA).

Exposure of NbNP to air causes their oxidation leading to the formation of niobium oxide nanoparticles (NbONP). The oxidation of NbONP was characterized with variety of techniques (XPS, EDS and HRTEM) that demonstrated the core-shell structure of the nanoparticles. These methods indicated that the core is metallic Nb^0 and the shell is the niobium oxide, Nb_2O_5. Since Nb_2O_5 is known be a strong Brønsted acid, we tested the Brønsted activity of NbONP with pH sensitive dye coumarin-6 (C_6) (monitored using fluorescence and UV-vis). The results of these spectroscopic experiments indicated that NbONP can protonate C_6, thus serving as confirmation for the acidity of NbONP. Furthermore, particles with varying sizes were tested with C_6 to check if the difference in size affects the acidity. It was observed that the particles with the larger sizes have the strongest acidity and the particles of smaller sizes are less acidic.

Acknowledgements

I was truly privileged to get opportunity to have Tito Scaiano as my research supervisor. I was able to not only study photochemistry, but to also perform research in the growing field of nanochemistry. Tito, thank you very much for all your help, support and patience! You are an inspiring role model for many scientists, and I feel really proud to be one of your students.

While being in the Scaiano group I was very fortunate to meet and work with variety of an amazing people. I would like to thank and acknowledge everyone with whom I have worked with throughout these years: Matt Decan, Kevin Stamplecoskie, Spencer Pitre, Greg Hodgson, Chiara Fasciani, Marco Mazzonna, Stefania Impellizzeri, Madeline Simpson, Chris Noel, Kater Peters, Hasitha deAlwis Weerasekera, Erika Wee, Adela I. Carrillo, Emilio Alarcon, Geniece Hallett-Tapley, Jose-Carlos Ferreira, Marisa Luisa Marin, Juliano A. Bonacin, Carlos J. Bueno, Mariana Vignoni, Natalia Angeluzzi Cunha, and Francisco Bosca.

Special acknowledgments goes to Michel Grenier (thank you for all your help with those pew pew), Hossein Ismaili ("What's the matter with you?"), Chris McTiernan (you are such a nice guy), Daniela Marquez Soto (Hello Kitty!), and Luciana Schmidt("lapicero! sí?"). Thank you all for your great sense of humor, your friendship and support. Importantly, I would like to say a vast thank you to my friend: Charles-Oneil Crites for helping me out in many lab situations during these years of research and study.

Also, a big thank you to Betty Yakimenko for all the help and keeping a great care in organizing our group!

I would like to recognize how great the department of chemistry is at uOttawa. I am very thankful that I was able to interact and meet with many remarkable graduate students and their research supervisors. I would like to acknowledge the following great individuals for their help and friendship: *Prof. Berezovski*, and his students Darija Muharemagic, Ana Gargaun, Gleb Mironov, Alexey Chechik; *Prof. Bryce*, and his students Kevin Burgess, Frédéric Perras, Jasmine Viger-Gravel; *Prof. Detellier* and his student Liva Dzene; *Prof. Richeson*; *Prof. Baker*; *Dr. Y. Liu* (SEM/TEM facility) and *S. Mommers* (XPS facility).

I would like especially thank Prof. Serge Gorelsky for all the help, advices and valuable discussions – it was a great fortune that we have met. I always keep in my mind your encouragements and mentorship, this department is very lucky to have you! Thank you!

Table of Content

Abstract iii
Acknowledgements iv
Table of Contents vi
List of Figures iii
List of Schemes v
List of Tables v
Abbreviations vi

1 • Introduction **8**

1.1 Objective 9
1.2 Hypothesis 13
1.3 Goals 15
1.3.1 Nanoparticles as Catalysts 15
1.3.2 Synthesis of Nanoparticles 18
1.3.3 Norrish type I reaction 20
1.3.4 Why Niobium? 26
1.4 Summary of Goals: *The theory of this work* 28
1.5 References 29

2 • Preparation of Niobium Oxide Nanoparticles: *Mechanistic Investigation* **31**

2.1 Photochemical Synthesis of NbNP 32
2.1.1 Conditions for Synthesis of NbNP 34
2.1.2 Irradiation of I-907 34
2.1.3 Niobium precursor 36
2.1.4 Air Sensitivity 39
2.1.5 Time of Irradiation 39
2.1.6 Effect of Irradiation on the growth of NbNP 43
2.1.7 Summary of conditions for synthesis of NbNP 44

2.2 Controlling the size of NbNP 45
2.3 Investigation of I-907 Photoproducts 49
2.4 MSBA and its Effects on the Growth of NbNP 52
2.5 Mechanism of the Growth of NbNP 56
2.5.1 The role of MSBA 56
2.5.2 Mechanism of NbNP growth using I-907 59
2.6 Experimental Details 62
2.7 Appendix 66
2.8 References 68
3 • Characterization of Niobium Oxide Nanoparticles: *Catalytic Investigation* **69**
3.1 Characterization of NbONP 69
3.1.1 Structural Analysis of NbONP 69
3.1.2 Amorphousness of NbONP (TEM and P-XRD) 69
3.1.3 Core-Shell of NbONP (HRTEM) 73
3.1.4 EDS Analysis of NbONP 75
3.1.5 XPS Analysis of NbONP 76
3.2 Catalytic properties of NbONP 82
3.2.1 Brønsted acidity of NbONP (Coumarin-6 dye) 82
3.3 Discussion and Summary 85
3.3 Experimental Details 87
3.4 Appendix (XPS results) 89
3.5 References 89
4 • NbONP as Sustainable Catalyst: *Scaling Up Synthesis* **91**
4.1 NbONP as a Powdered Catalyst 92
4.2 Scaling up – Reaction Apparatus 93
4.3 Limitations 96
4.4 Experimental Details 97
5 • Conclusion: *Future Directions* **99**
5.1 Summary 100
5.2 Future Studies 99
5.3 Publications Resulting from Work Presented in this Thesis 103

List of Figures

Figure 1.1 The UV-Vis spectrum of spherical gold nanoparticles in water with an absorption maximum at 525 nm. Orange curve (─) represents a theoretical scattering plot that is typically found for the most colloidal particles that do not possess any plasmon mode within their absorbance region. The blue curve (─) represents a theoretical peak for how the actual resonance plasmon mode would look like if the scattering had not been present. The red curve (─) is an absorbance of AuNP with a 15 nm mean size, prepared using a photochemical approach (this synthesis are further described in section 1.3.2). 10

Figure 1.2 Formation of the surface plasmon resonance by interaction of light with the surface of AuNP. Upon electron excitation, surface charge polarization occurs that causes dipole formation. . 11

Figure 1.3 Comparison of the sizes of nanoparticles to the percentage of surface atoms available. As the size decreases, the percentage of surface atoms increases. 16

Figure 1.4 Theoretical representations of 2 and 5 nm cubeoctahedron crystal surface of gold nanocluster. The corner atoms depicted in dark have been reported to possess the highest catalytic activity.[12] 17

Figure 1.5 The seed mediated growth mechanism for formation of metallic nanoparticles (e.g. AuNP). After the reduction of metallic cations, metal atoms bond together to form seed clusters. These seeds continue to grow until their surfaces are stabilized by available ligands. Ligands also protect the particles from agglomeration. 19

Figure 2.1 Absorbance spectrum of 190 µM solution of I-907 in acetonitrile during photoexcitation with UVB light.[4] 34

Figure 2.2 Raman spectra of ethanol (—), $Nb(acac)_5$ in acetonitrile (—), acetylacetone in acetonitrile (—) and $Nb(OCH_2CH_3)_5$ in acetonitrile (—). 37

Figure 2.3 Absorption spectra during UVB irradiation of I-907 (190 µM) and $Nb(acac)_5$ (10 µM) in acetonitrile.[4] 40

Figure 2.4 Formation of NbNP after 10 minutes (A), 30 minutes (B), 60 minutes (C) and 300 minutes (D) of UVB irradiation as examined by TEM. 41

Figure 2.5 Enlargement of NbNP diameter during photoirradiation. NbNP sizes were calculated using a mean of 100 individual nanoparticles. 42

Figure 2.6 Absorbance of 190 µM I-907 and 10 µM $Nb(acac)_5$ in acetonitrile after UVB irradiation for 10 minutes, followed up by placing the sample in the dark until 300 minutes.[4] 43

Figure 2.7 Size distribution of two NbNP samples obtained from solutions with 60 µM (red) and 620 µM (blue) concentrations of I-907. Insets depict TEM images of the samples.[4] 45

Figure 2.8 TEM analysis (left) and its related size distribution histograms (right) of NbNP prepared from solutions with 10 µM $Nb(acac)_5$ and (a) 60 µM, (b) 80 µM, (c) 100 µM, (d) 190 µM, (e) 260 µM, (f) 420 µM, (g) 520 µM, (h) 620 µM and (i) 730 µM I-907.[4] The size bar corresponds to 200 nm in each of TEM images. 46

Figure 2.9 NbNP mean diameters obtained after 300 minutes irradiation of solutions containing 10 µM $Nb(acac)_5$ and varying concentrations of I-907. NbNP sizes were calculated from an average of at least of 100 individual nanoparticles. 47

Figure 2.10GC analysis of (A) 190 μM I-907, (B) 190 μM MSBA, (C) 190 μM isopropylmorpholine and (D) a solution of 190 μM I-907 after 60 minutes of UVB irradiation (in CH_3CN solution and under argon).....49
Figure 2.11 (1) Photodecomposition of I-907 into two types of radicals (2) Major photoproducts of I-907 irradiation: MSBA and ISOMOR.....50
Figure 2.12 Photodecomposition of MTB into two types of radicals: Benzoyl and α-hydroxy radicals. While α-hydroxy radical acts like an excellent reducing agent in polymerization, the benzoyl radical spontaneously forms into MSBA.....51
Figure 2.13 Variation in NbNP mean size for samples with 10 μM $Nb(acac)_5$ and 60 μM I-907 that had been UVB irradiated for 5 minutes and followed by the addition of 560 μM MSBA or ISOMOR. The data of 620 μM I-907 was included for size comparison. T-test statistical analysis demonstrated the statistical data difference ($p < 0.001$) in all of the cases.....52
Figure 2.14 UVB irradiation of 190 μM MSBA and 10 μM Nb(acac)5 in CH_3CN under argon.[4].....53
Figure 2.15 Represents TEM images of samples containing 10 μM $Nb(acac)_5$ and (A) 60 μM, (B) 190 μM and (C) 520 μM MSBA. From the average sizes (represented to the left of each image), it was found that the diameter of NbNP increased correspondingly with the MSBA concentration increase.....55
Figure 2.16 GC analysis of 190 μM MSBA after 60 minutes of UBV irradiation (all performed in CH_3CN and under argon). (MS results for this GC analysis are displayed in Appendix 2.7).....56
Figure 3.1 TEM of NbONP prepared from a solution of 420 μM I-907 and 10 mM $Nb(acac)_5$. Inset depicts diffraction pattern of these particles using SAED.....72
Figure 3.2 P-XRD pattern of NbONP as powder, prepared from a solution of 420 μM I-907 and 10 mM $Nb(acac)_5$.....73
Figure 3.3 Graphic representation of the surface oxidation of NbNP (left). Representative HRTEM image of NbONP (420 μM $Nb(acac)_5$ and 10 mM I-907) depicting a rough 5-10 nm Nb oxide shell (right).....74
Figure 3.4 EDS analysis of NbONP (420 μM $Nb(acac)_5$ and 10 mM I-907). Note the results on atomic % for O and Nb, (5/2), confirming Nb_2O_5 formation on the particles` surface.[5].....75
Figure 3.5 Graphical representation of XPS sputtering of NbONP powder prepared on the silicon wafer (420 μM $Nb(acac)_5$ and 10 mM I-907).....76
Figure 3.6 XPS spectra of NbONP (420 μM $Nb(acac)_5$ and 10 mM I-907) before and after ionic sputtering.[5] Note the formation of peaks of Nb^0 after the sputtering took place.....77
Figure 3.7 XPS spectra of commercial Nb_2O_5 catalyst (obtained from CBMM, Brazil) before and after ionic sputtering.[5] Note the lack of Nb^0 after sputtering.....79
Figure 3.8 XPS analysis of 1s C region of NbONP (420 μM $Nb(acac)_5$ and 10 mM I-907) before sputtering.....81
Figure 3.9 Fluorescence emission spectrum of a 0.9 μM C_6, control (Δ), 0.9 μM C6 in the presence of 91 fM (□) and 0.4 pM (○) NbONP. NbONP were prepared using 260 μM I-907 and 10 μM $Nb(acac)_5$. Addition of C_6 into solutions NbONP resulted in an immediate decrease in the intensity of C6 emission (λemit = 500 nm, λex = 450 nm). Inset presents an increase in emission at λemit = 555 nm (λex = 520 nm) of the C6 protonated form (HC6+).[5].....83
Figure 3.10 UV-Vis absorption spectra obtained for the samples containing 0.9 μM of C6 with (1) 0 nM, (2) 91 fM and (3) 0.4 pM of 85 ± 15 nm NbONP. Three areas are highlighted to represent the major, light-absorbing species in the reaction: (a) NbONP (light scattering), (b) non-protonated coumarin-6, and (c) protonated C_6.....84
Figure 4.1 Graphical illustration of designed apparatus (left), where 100 mL of prepared solution is being kept under the inert atmosphere. Inset on the right is an actual picture of this set-up with the three UVB panels surrounding it (to the total of 15 UVB lamps).....94
Figure 4.2 TEM image of NbONP powder prepared using the scaled up method from the solution of 420 μM Nb(acac)5 and 10 mM of I-907.....95

App. Figure 1.1 Mass spectrum of 4-(methylthio)benzoic acid (MSCOOH).....66
App. Figure 1.2 Mass spectrum of 4-(methylthio)benzaldehyde (MSBA). 66
App. Figure 1.3 Mass Spectrum of benzaldehyde (BA).....67

List of Schemes

Scheme 1.1 Mechanism of generating a radical pairs from the irradiation of pinacolone with a light. The two radicals can undergo either a combination or disproportionation. 21
Scheme 1.2 Formation of radical pairs - generated from the irradiation of Irgacure 2959 with a light. The produced ketyl radicals transfer their electrons to the gold cations, which are reduced to Au^0 and gold nanoparticles are formed.[15].....22
Scheme 2.1 Photochemical sequence into the synthesis of NbNP that leads into the formation of NbONP. 33
Scheme 2.2 Illustrates a formation of reported photoproducts from UVB irradiation of MSBA in solution of CH_3CN under argon. Note: the solvent CH_3CN is contaminated with the traces of water. Formation of MSCOOH is most likely due to the traces of O_2, hence the smallest intensity for the GC peak. 57
Scheme 2.3 Proposed mechanism for the growth of photochemically generated NbNP. 60

List of Tables

Table 1.1 Quantum yields and triplet nature for α-cleavage of ketones (1-6). 24
Table 3.1 Mean size of NbONP and their acitivity on Protonation of Coumarin-6 dye.....82
Table 3.2 Combined data of XPS analysis. 89

Abbreviations

Φ_f	fluorescence quantum yield
µM	micromolar
ACN	acetonitrile
AgNP	silver nanoparticles
AuNP	gold nanoparticles
BA	benzaldehyde
BP	benzophenone
CuNP	copper nanoparticles
GC	gas chromatography
hυ	photon of light
I-2959	Irgacure 2059, Ciba®
I-907	Irgacure 907, Ciba®
L	liter
LC	liquid chromatography
LED	light-emitting diode
LFP	laser flash photolysis
MSCOOH	4-(methylthio)benzoic acid
MSBA	4-(methylthio)benzaldehyde
mp	melting point
mM	millimolar
MS	mass spectrometry
Nb^{+5}	niobium (V)

NbONP	niobium oxide nanoparticles
NbNP	niobium nanoparticles
NMR	nuclear magnetic resonance
ppm	parts per million
R•	carbon centered with radical
SEM	Scanning electron microscopy
SPR	surface plasmon resonance
pM	picomolar
TEM	transmission electron microscopy
T	temperature
UVA	ultraviolet radiation range is from 315-400 nm.
UVB	ultraviolet radiation range is from 280-315 nm.
UVC	ultraviolet radiation range is from 100-280 nm.
UV-vis	ultraviolet-visible
UV	ultraviolet

1 • Introduction

"Just wait - the next century is going to be incredible. We are about to be able to build things that work on the smallest possible length scales, atom by atom. These little nanothings will revolutionize our industries and our lives" [1, 1b]

Richard Smalley, Nobel Laureate

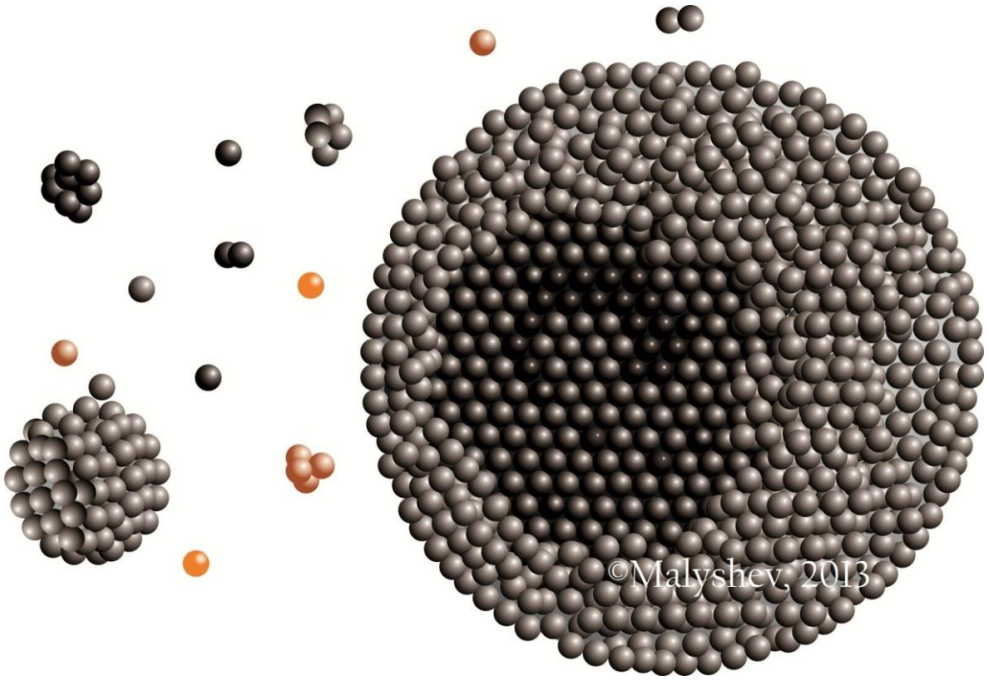

Cover Image designed and created by Dimitriy Malyshev.

1.1 Objective

Nanochemistry, as a highly expanding industrial field, has not just received tremendous success from the scientific community, but has also generated great perspective for the economic development in countries, such as Canada. It is matter manipulation at a nanoscale that allowed miniaturization of new devices, which then caused a vast impact on the development in electronics and medicine. However, as much as it is exciting to hear about technological innovations that came from the field; what it really brought within the academia is a new paradigm shift[2] - a broader method in solving problems. This brings us to the theoretical objective of this thesis: *to make a shift from a traditional scientist's mindset and develop a new mental flexibility in the design of solutions to problems at a nanoscale.*

Without any doubt nanochemistry is an interdisciplinary field that combines traditional fields of chemistry and solid-state physics.[3] It has been said that it exists within the dimensional gap of 1 nm to 100 nm, where neither quantum chemistry (<1 nm) nor classical law of physics (>100 nm) may hold.[1b] In that nanoscale regime when a strong chemical bonding is present a unique delocalization of valence electrons may occur. However, the extent with which those electrons may delocalize become a strongly size dependant effect.

That is, for any "nano-effect" to take place we need to downsize the bulk matter in order for it to accumulate those new changes, such as surface reactivity, conductivity, melting points, magnetic and optical properties.[4] The classical example for this nano-effect could be best illustrated by observing the change in the color of gold. In its bulk structure gold exhibits a bright yellow color, but when colloidal nanosized particles are prepared in aqueous solution (within an

average size of 15 to 20 nm) the appearance of color changes to the pink-red.[4] Such change in color is directly proportional to the ability of these particles to absorb the light as energy, as seen in the UV-vis spectrum of **Figure 1.1**.

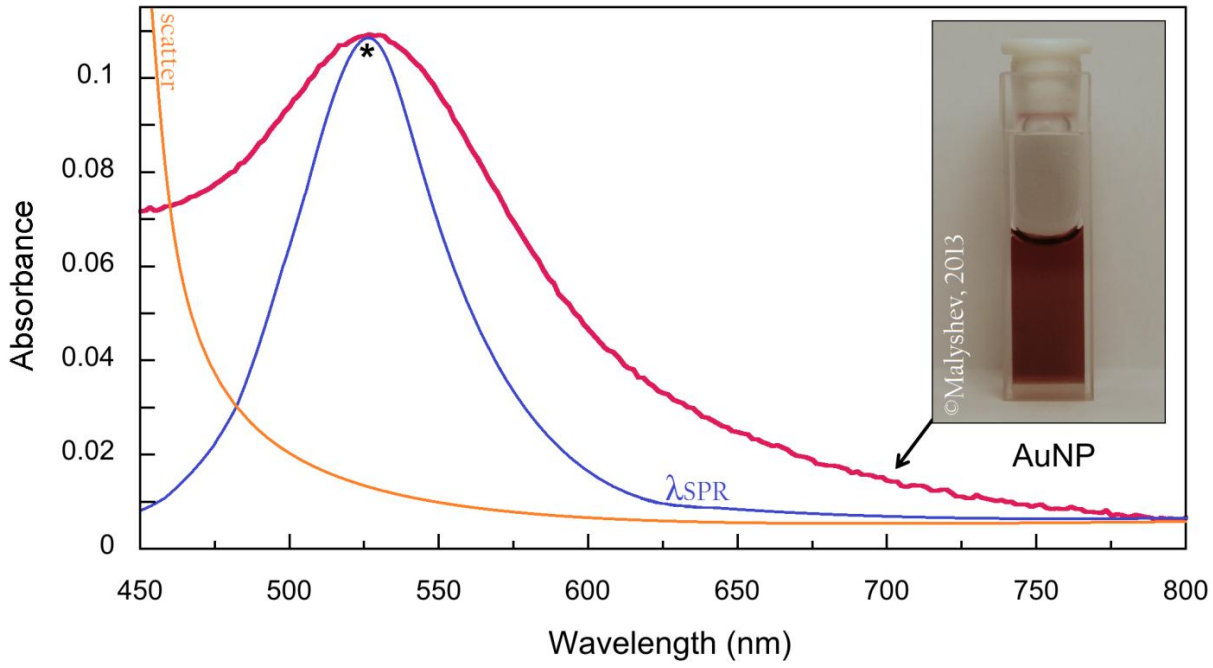

Figure 1.1 The UV-Vis spectrum of spherical gold nanoparticles in water with an absorption maximum at 525 nm. Orange curve (—) represents a theoretical scattering plot that is typically found for the most colloidal particles that do not possess any plasmon mode within their absorbance region. The blue curve (—) represents a theoretical peak for how the actual resonance plasmon mode would look like if the scattering had not been present. The red curve (—) is an absorbance of AuNP with a 15 nm mean size, prepared using a photochemical approach (this synthesis is further described in section 1.3.2) .[5]

Absorbance bands of solutions of gold nanoparticles (AuNP) are due to the phenomenon known as the plasmon resonance, which is described by the Mie theory.[2] According to this theory the absorbance of nanoparticles may be expressed using two conditions: the *light scattering* and *dielectric constants* of both metal and its surrounding medium. Therefore, (without going deeper into mathematical details) the result of these two phenomena is what gives rise to the actual absorbance spectrum of AuNP. As we look into the details of **Figure 1.1**, we could see how the scatter from the particles affects the spectrum by broadening the absorption band. However, it is only when we subtract the scattering effect from the measured spectrum that we are able to see a distinctive absorbance band from the plasmon resonance. A physical description of the plasmon resonance is depicted in **Figure 1.2.**

*Figure is designed and created by Dimitriy Malyshev.

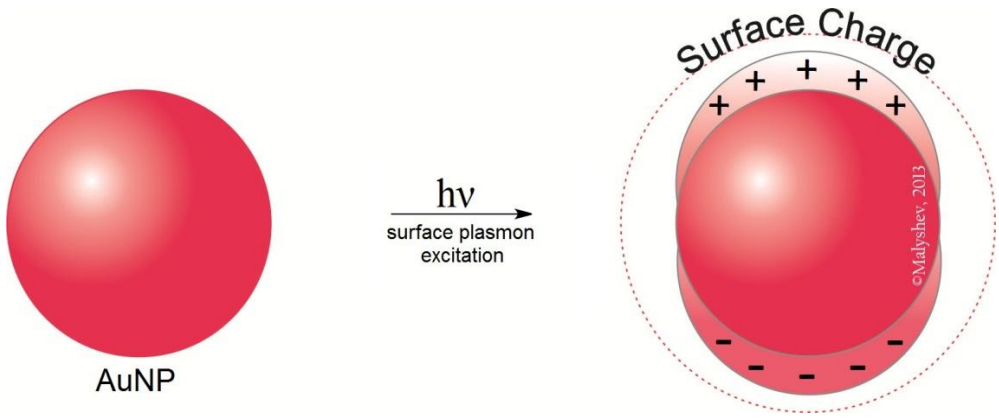

Figure 1.2 Formation of the surface plasmon resonance by interaction of light with the surface of AuNP. Upon electron excitation, surface charge polarization occurs that causes dipole formation.

When the particle interacts with visible light, the electron cloud of the nanoparticle responds to it: the new electronic state is generated and the electron distribution is perturbed. An electron oscillation creates surface polarization and causes the formation of a dipole. The dipole of the particle is what ultimately causes appearance of a resonance at a specific wavelength.[2] When the particles are not spherical but elongated, two dipole oscillation modes are possible: one along the transverse and the other along longitudinal axis. Therefore, when two different dipoles are formed, two plasmon bands are expected in the absorption spectrum. Metal nanoparticles of gold, silver and copper are well known to possess such plasmon resonances in the visible region, but for nanoparticles of most other metals the plasmon bands occur in the UV region and cannot be easily detected.

In brief, we touched upon an important theme of how physical size can influence the properties of the matter. After this introduction to the gold nanoparticles, we will use them further in this chapter, as a paradigm for synthesis of niobium nanoparticles.

1.2 Hypothesis

It has been well established in the literature that the novel properties of nanomaterials are indeed dependent on their relative sizes, but the majority of the literature reports describe materials that do not fall under the earlier stated definition of nanochemistry – their sizes are not between 1 to 100 nm. Thus, it is within the shared hypothesis of many scientists[3, 6] that nanochemistry, as a term, should not be restrained by strict definition of the stated dimensions, but be instead *referred to the systems whose properties vary with size*. Such flexibility to the term shall allow one to expand the dimensional gap (to below 1 nm and to above 100 nm) as long as property of studied material is indeed dependent on size.

There are two major schematic approaches to the synthesis of nanomaterials, *top-down* and *bottom-up*. In its earlier days the majority of nanodevices utilized a top-down approach as their primary method of fabrication. One of the best known types for the top-down approach is a lithographic etching of the silicon semiconductor.[6] This method was pivotal in the development of modern computer chips. Nowadays, modern ways of processing such as plasma processing, allow smaller (with the least amount of defects) and reliably resolvable features to be made (sized to 22 nm).[7] Obviously, it is a great achievement compared to the 2000 nm chip components created over a decade ago,[6] but with a desire to further push the limits of Moore's law (a major force for integrated circuits innovation) and to go below 32 nm (reported resolution, but with high heat and defect issues[7]) a growing appeal of methodology goes towards the *bottom-up* approach.[8]

Going bottom-up or in other words synthesizing up is becoming an important theme in the development of nanomaterials. Primarily this method involves a use of chemicals and preparation of materials in "wet" chemistry labs where sometimes reaction with oxygen and water could be unavoidable in affecting the final structural outcome of the material.[1b] Significantly, it becomes an important aspect in research to develop new synthetic approaches and suitable laboratory equipment to synthesize a good monodispersed material. Given these points, we may sum up by stating the primary hypothesis for this thesis: *higher dimensional control may be achieved by using a bottom up approach and this method should be used as a synthetic method for the synthesis of nanomaterials, even under the wet chemistry lab settings.*

1.3 Goals

1.3.1 Nanoparticles as Catalysts

For the most part, it is well accepted that the bottom-up approach should be replacing the classic top-down one. Certainly nothing represents a bottom up approach better in nanochemistry than the synthesis of nanoparticles in solution. Conceptually, nanoparticles are very simple. They are small, spherical and have a radius within the range of 1 to 200 nm. Nanoparticles are often found to be very monodispersed, but that is directly dependant on the synthetic method that is being utilized. In general, they can be synthesized from any material, although metallic nanoparticles carry the most interest in research and are particularly well studied. Synthesis of nanoparticles from noble metals, such as palladium or rhodium is specifically studied for their ability to act as a heterogeneous catalyst.

There is no doubt that the development of homogenous catalysts takes up a large proportion of academic research. They are highly selective and are very efficient, but they do possess disadvantages, such as low thermal stability and difficulty of isolating them from the solution after the reaction is complete.[9] Conversely, heterogeneous catalysts can be easily removed from the reaction mixture, and moreover they are proven to be highly thermally stable.

Despite missing the selectivity of homogenous catalysts, heterogeneous catalysts are in demand due to their environmental friendliness. They fall into the category of a “green catalyst”, primarily due to the efficiency of being recyclable and re-usable. Often times “green” are also referred to catalysts with a low toxicity, but it strictly dependable on the type of metal and material that are being used. Not all of the heterogeneous catalysts are completely non-toxic.

In context, nanoparticles are classified to be heterogeneous catalysts for they primarily utilize metallic surfaces to perform catalysis. But, compared to the bulk metals they have unique capacity to increase a proportion of surface atoms as they decrease in size. For instance, a 2 nm metallic particle has 90% of its atoms on the surface, while a 4 nm particle has 70%, and only 50% of atoms are available for a 6 nm particle, **Figure 1.3**.[10]

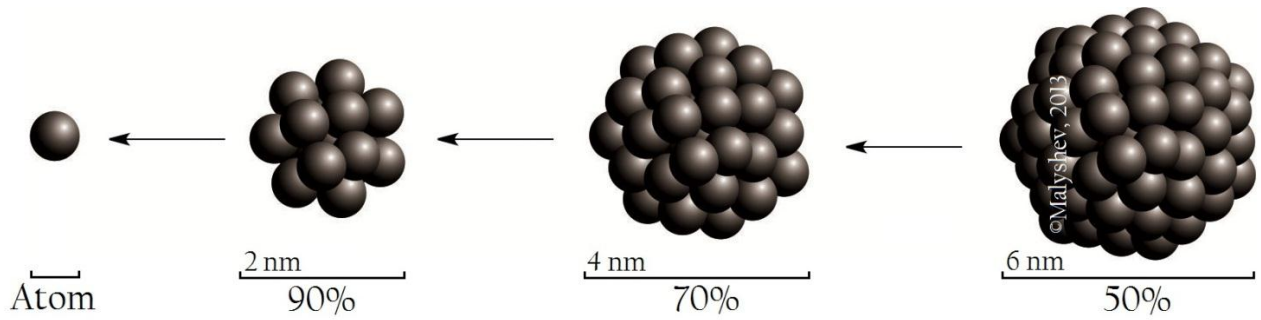

Figure 1.3 Comparison of the sizes of nanoparticles to the percentage of surface atoms available. As the size decreases, the percentage of surface atoms increases.

From the illustration above, if most of atoms are located on the surface of a particle, then the higher number of atoms is expected to be active during catalysis. In fact, if we were to choose between synthesize of two group sizes of particles that of 2 nm and of 6 nm in diameter, then it is favourable to synthesize particles of 2 nm size for it will generate a higher catalytic surface area. In essence, the above behavior applies to the nanoparticles of both crystalline and amorphous states. However, studies with the crystalline gold cubooctahedral have demonstrated that, among available surface atoms, atoms at edges and corners are most active in catalysis, **Figure 1.4**.[9,3]

*Figure is designed and created by Dimitriy Malyshev.

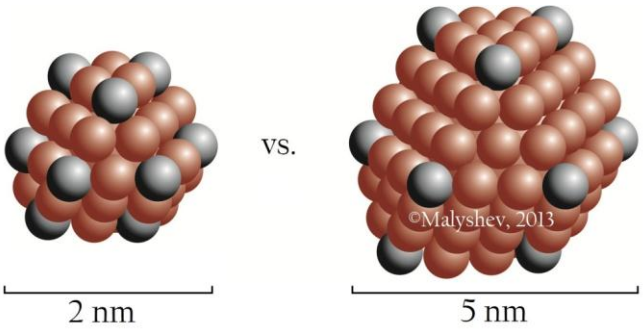

Figure 1.4 Theoretical representations of 2 nm and 5 nm cubooctahedral crystal surface of gold nanocluster. The corner atoms depicted in dark have been reported to possess the highest catalytic activity.[11]

A surface of the cubooctahedral particle contains three type of atoms: atoms on the faces, edges and corners (note that the number of metal atoms on each edge is the same for a given cubooctaheron). The studies of the mechanism of CO oxidation (the most well studied reaction for Au cubooctaheron particles) determined that the low-coordinated corner sites are the active sites and the catalytic activity of the nanoparticles increases with the number of the low-coordinated atoms in these structures.[12] It is natural to assume that valence-unsaturated atoms in nanoparticles from other metals will exhibit similar increased activity. The majority of particles with high catalytic activity are only few nanometers in diameter.[9,13]

What makes nanoparticles so much different from traditional heterogeneous catalysts is their ability to be soluble in solvents in the form of colloids. Nanoparticles stay in solution due to their high surface stabilization and motifs such as ligands, surfactants, polymers and silicon shells all interact with the surfaces of particles – keeping them within the liquid phase. This ligand surface stabilization may be of disadvantage to catalysis, as the ligands may block access to catalytically active sites of nanoparticles.[1b]

1.3.2 Synthesis of Nanoparticles

Nanoparticle may refer to either a crystalline or amorphous solid state structure. Formation of either of these states is strongly dependant on the conditions that are being used during synthesis. Variable factors, such as temperature, time, stirring, and the type of solvent with reducing agents all play important roles.

Popularly adapted synthetic strategies for the preparation of nanoparticles involve reduction of positively charged metal atoms, such as ions or an organometallic complexes.[4] The choice of reaction media becomes a dependable feature not just on the type of ions and reducing agent that are being used, but on the final geometry of nanoparticles.[2] Typically, solution may vary either from a highly polar (e.g. water) to a non-polar (e.g. benzene) solvent.[1b]

Such salt reduction methodology was first utilized by Brust and Schiffrin in the early 1990s for the synthesis of gold nanoparticles. Their procedure involves reduction of $HAuCl_4$ by $NaBH_4$ in toluene with the presence of tetraoctylammonium bromide, as a surfactant ligand. **Figure 1.5** illustrates a seed mediated mechanism of the formation of the nanoparticles, where the following two consecutive conditions must be met for success:

i) Concentration of reducing agent is stoichiometric to the amount needed for the reduction of metal cations to the zero-valent state.

(e.g: Au^{3+} requires three equivalents of $NaBH_4$ to reduce Au^{3+} to Au^0).

ii) Suitable surfactant molecules or lipophilic ligands must be present to control the particle growth and to prevent agglomeration.

*Figure designed and created by Dimitriy Malyshev

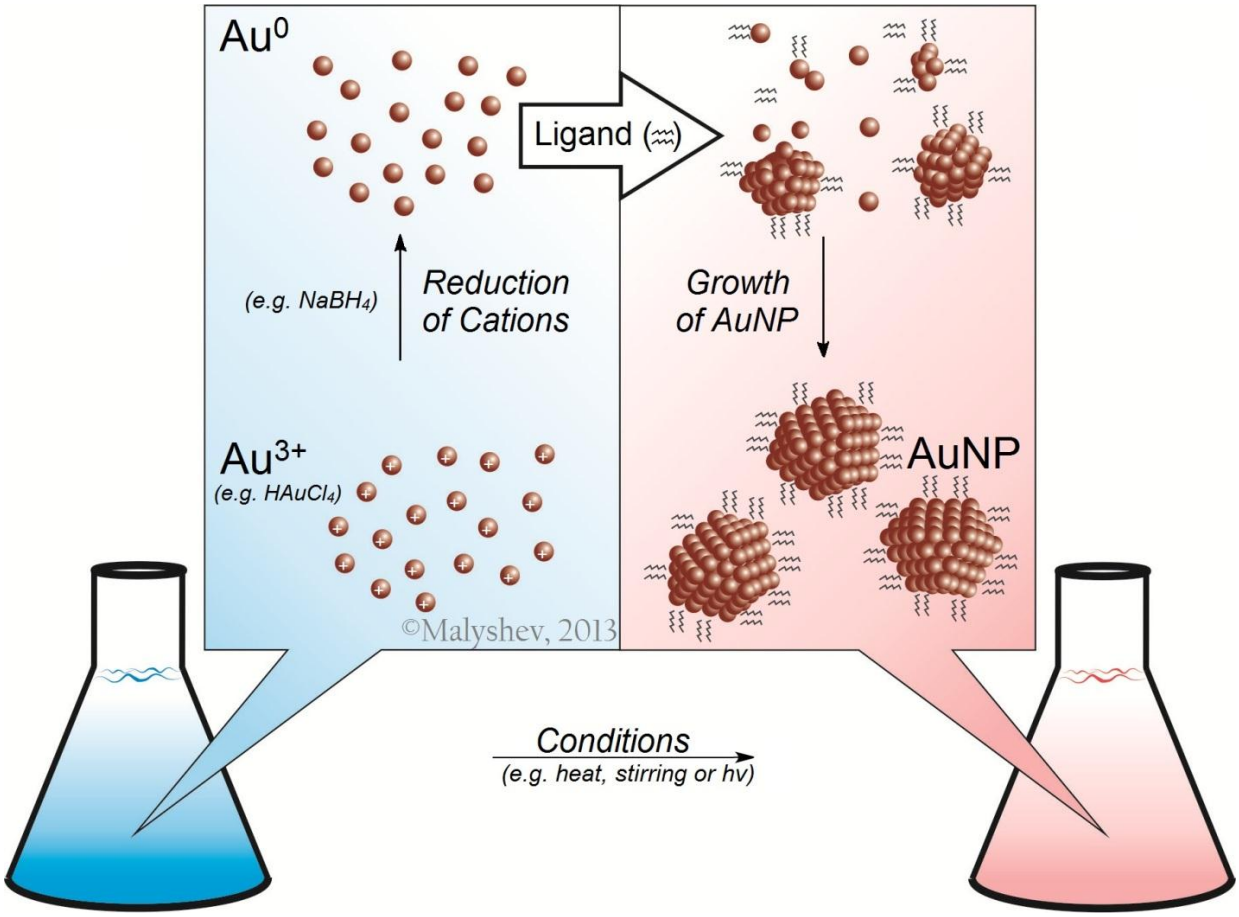

Figure 1.5 The seed mediated growth mechanism for formation of metallic nanoparticles (e.g. AuNP). After the reduction of metallic cations, metal atoms bond together to form seed clusters. These seeds continue to grow until their surfaces are stabilized by available ligands. Ligands also protect the particles from agglomeration.

When a solid is suspended within a liquid solvent without causing its precipitation, we refer to such two phase mixture as colloidal. Indeed, nanoparticles are true colloids if they remain in the solution and do not precipitate. This is because nanoparticles are not just very small in size, but they are also highly stabilized by the ligands on their surfaces. These ligands act as coating groups that protect particles by sterically hindering their surfaces from each other, thus preventing agglomeration and enhancing their solubility.[6] Furthermore, surfactants guide particles growth and been used as method of control over the size and their monodispersity. In fact, if the ligands are already present in solution when the reduction is initiated, it prevents the growth of large particles. But, when the ligands are added subsequently it is difficult to obtain desired size unless an exact moment is known (a stage of cluster formation). [1b,9]

1.3.3 Norrish type I reaction

Over seventy years ago, Norrish and Appleyard discovered that upon irradiation of a ketone with the light, the weakest of its two α-C-C bonds may undergo a cleavage.[14] Nowadays, α cleavage of carbonyl compound is referred to as a Norrish type I reaction. For example, in **scheme 1.1**, we depict that the breakage of α-C-C bond in **1**, pinacolone (3,3-dimethyl-2-butanone), leads to the formation of two radical pairs; the acyl and *tert*-butyl radicals.[15] Although, both of the resulting radicals may undergo combination or disproportionation, it is the understanding of the mechanism of their products formation that becomes applicable in the development of new applications. [15]

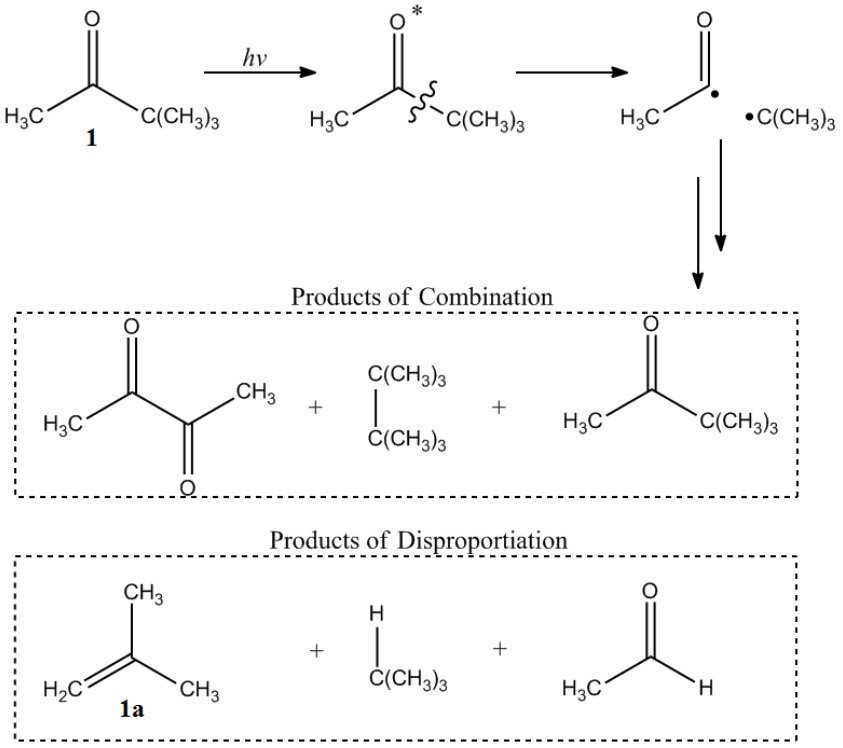

Scheme 1.1 Mechanism of generating a radical pairs from the irradiation of pinacolone with a light. The two radicals can undergo either a combination or disproportionation.

Specifically, one of the products of disproportionation of *tert*-butyl radical is isobutylene, **1a**. Such products may only be formed in a transformation which involves two steps: an electron transfer and a follow-up proton transfer. Each of these steps are described by Mayer within the well-established theories of proton and electron transfer.[16,17] In fact, this ability of a carbon centred radical (R•) to transfer an electron had created a new paradigm in the synthesis of nanoparticles. In particular, our laboratory has developed a methodology to utilize photoinitiators from the Norrish type 1 reaction for the formation of gold nanoparticles, as seen in **scheme 1.2**.[18]

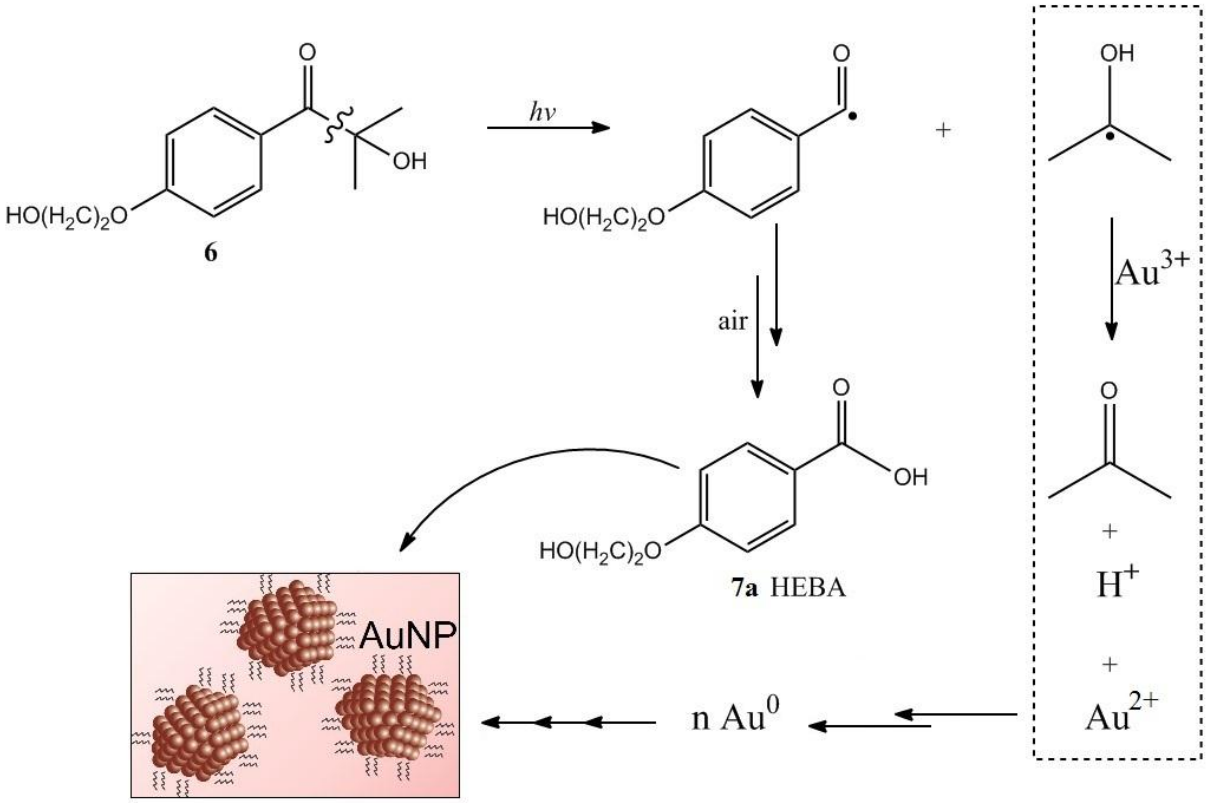

Scheme 1.2 Formation of radical pairs - generated from the irradiation of Irgacure 2959 with a light. The produced ketyl radicals transfer their electrons to the gold cations, which are reduced to Au0 and gold nanoparticles are formed.[15]

Upon irradiation of Irgacure-2959 (**6**), the benzoyl and the acetone ketyl radicals are formed (**scheme 1.2**). This photochemical splitting of the α-C-C bond in **6** is also governed by the Norrish type 1 mechanism. However, rather than letting these radical products undergo a recombination or disproportionation, metallic cations of noble metals (Au, Ag and Cu) promote an alternative reaction pathway. These cations are mild oxidizing agents and can abstract electrons from the ketyl radicals.[18] Thus, reduction of the metal atoms occurs, zero-valent metal

atoms form clusters and grow into nanoparticles. Furthermore, it has been demonstrated that the benzoyl radical does not participate in an electron transfer, but instead reacts readily with dioxygen (*via peracid*) to form the benzoic acid **7a,** HEBA. [18] Interestingly, **6a** displays an important role as an active ligand during the formation of nanoparticles. The role of **6a** as a surface stabilizer has been confirmed in an experiment in which an addition of **6a** into the solution of gold nanoparticles, synthesized via the traditional method, stabilizes their size and growth. [18]

Irgacure-2959 as the photoinitiator in the synthesis of gold and silver nanoparticles has been used with success.[19] The ability of Irgacure-2959 to generate radicals and to reduce the metallic cations is due to the favorable process of the cleavage of the α-C-C bond in the $n\pi^*$ excited state.[18] Irradiation of the Pinacolone (**1)**, allows generation of the radical pairs with the quantum yield of 0.33. [15] Such cleavage of the α-C-C bond in **1** is driven by the stability of radical pairs that are being formed. While the formation of tert-butyl radical is favorable, the absorbance coefficient of **1** is low. Furthermore, **1** is not a good electron donor, the desirable property that is required in this work.

Table 1.1 Quantum yields and triplet nature for α-cleavage of ketones (1-6).

Name and Structure	Φ_α[a]	Triplet Nature
1 (Pinacolone) 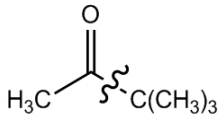	0.33[b]	$n\pi^*$
2 (Pivalophenone) 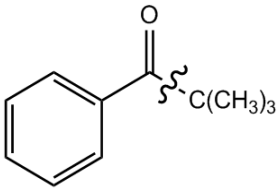	0.30[b]	$n\pi^*$
3 (Photocure 1173) 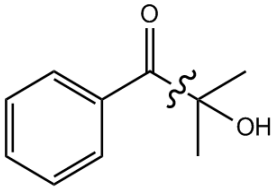	0.38[c]	$n\pi^*$
4 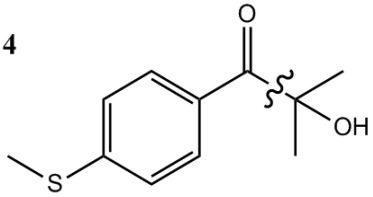	0.01[c]	$\pi\pi^*$
5 (Irgacure 907) 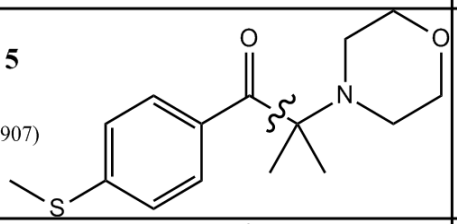	0.25[d]	$n\pi^*/\pi\pi^*$
6 (Irgacure 2959) 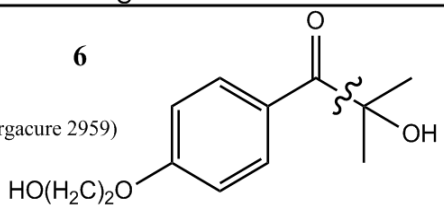	0.29[c]	$n\pi^*/\pi\pi^*$

(a) Φ_α – quantum yield, (b) Ref.[15], (c) Ref.[20] (d) Ref.[21]

To increase the light absorbance of **1** and to increase its quantum yield we can modify the methyl group of the acetyl by substitution with the phenyl group. However, even with an increased absorbance coefficient, the resulted structure **2**, has no increase in the quantum yield and, in fact, a small decrease is observed (**Table 1.1**). This can be explained by noting that the triplet excited state of **2** possess some $\pi\pi^*$ character from the phenyl group.

For molecules with the $n\pi^*$ triplet state, the α-C-C bond cleavage occurs faster when photogenerated by-products can stabilize the radical formation. We can apply a captodative effect, which involves the stabilization of radicals with electron-withdrawing (EWG) and electron donating (EDG) group substituents during their free radical formation.[15] For example, derivatization of **2** with the hydroxyl EDG produces **3** which has a higher quantum yield than **2**.[20] Upon irradiation, **3** generates an acetone ketyl radical that is capable to be electron donor. However, further modification of **3,** with the introduction of EWG methyl sulfate into the phenyl results in the decrease of its quantum yield (structure **4**). This is because **4** has a $\pi\pi^*$ triplet state. To change the $\pi\pi^*$ character of the triplet state, a structure should be modified by the substitution of hydroxyl group with stronger EDG, as shown in the structure of **5** (Irgacure 907 (I-907)).

The triplet state of I-907 has both $n\pi^*$ and $\pi\pi^*$ character. Such mixed character gives not only the higher quantum yield, but also produces an α-amino alkyl radical (further details, see **Chapter 2**). The α-amino alkyl radical of I-907 is a stronger reducing agent than the acetone ketyl radical of I-2959.[22] Since, I-907 and I-2959 are both excellent choices for the synthesis of nanoparticles (as was demonstrated with Au, Ag and Cu), it is the goal of this work to test both of these photoinitiators for the synthesis of nanoparticles of niobium, a different type of metal that previously has not been used.

1.3.4 Why Niobium?

Niobium is very oxophilic.[23] It possesses a range of oxidation states (from +5 to -1), but primary found in the highest oxidation state (+5). Despite the fact that organometallic chemistry of niobium is rich, majority of its research has been focused on the solid-state chemistry. High electrical conductivity and resistance to corrosion makes niobium suitable for use in many applications. Currently, niobium is used in the production of superconducting magnets, capacitors, and (importantly) heterogeneous catalysts.[23]

Niobium(V) oxide is an air-stable and insoluble solid. The color of Nb_2O_5 is white, however upon heating (with the Bunsen flame) the color changes to yellow due to the formation of oxygen defects in the lattice. This yellowing reverts itself upon cooling. The crystal structure of Nb_2O_5 is complicated and possesses a strong polymorphism. Niobium(V) oxide have been reported to be amorphous until it is being calcined to 773 K, where it then begins to crystalize. [23]

If niobium oxide react with water, niobic acid [$HNbO_3$] is formed. This acid has a high strength (H_o = -5.6) and contains both Lewis and Brønsted acid sites. While being highly abundant on its surface with the Brønsted acid sites, niobic acid loses them upon heating (the complete loss at 800 K). The opposite affect is observed for the Lewis acid sites: their abundance are increases as the temperature goes up (up to 773K).[23] Consequently, when niobic acid is in its amorphous state it is rich with the Brønsted acid sites, but upon its treatment with the heat it changes into the crystalline state that forms Lewis acid sites from the existed Brønsted acid sites.[24]

Niobic acid can act as an effective catalyst for reactions in water or in reactions in which water molecules are involved. For example, 10 wt % of Nb_2O_5 (supported on silica-alumina) catalyzes the esterification of acetic acid with a variety of alcohols.[25] In all of these performed reactions there is 100% selectivity with an excellent conversion for ethyl (83%), *n*-butyl (87%), and isopenytyl (91%) acetates.[25] In another example, 23 wt % of Nb_2O_5 (supported on silica) catalyzes the epoxidation of cyclooctene with H_2O_2, where the high stability of catalyst was demonstrated and allowed its further reuse. [26]

The important goal of this work is to demonstrate that the acidity of niobic acid is not limited to its usage as a bulk heterogeneous catalyst, but can be effectively employed in nanoparticles. Nanoparticles have higher surface area and thus should exhibit stronger reactivity compared to heterogeneous catalysts.

1.4 Summary of Goals: *The theory of this work*

Following the success for synthesis of nanoparticles (Au, Ag and Cu) using Irgacure photoinitiators (I-2959 and I-907), we will use these molecules in the synthesis of niobium nanoparticles (NbNP). The synthesis of NbNP will then be investigated with the study of the mechanism of nanoparticle formation (Chapter 2). The investigation techniques will involve the use of UV-Vis absorption spectroscopy and GC-MS spectrometry.

The results of this mechanistic study and the data on particles sizes will then be compared to the findings from the literature. Ideally, the goal is to be able to have the full control over the size of generated NbNP. Such control over the particles' size will allow development of a library of NbNP with varying sizes, which will then be used to explore how the decrease in size affects the acidity of NbNP (Chapter 3).

The major portion of this work is characterization of NbNP's structure (Chapter 3). Knowledge of its oxide and crystal states will allow us to predict the type of acidity (Brønsted or Lewis) that NbNP possess. Techniques such as P-XRD, EDS, and XPS were utilized during the characterization. Upon identification of the nature of an acid, a molecular sensor (such as Coumarin 6 dye) used to test the acidity, monitored using Fluorometric and UV-vis spectrometry. The final portion of this research focuses on the scaling up synthesis for the production of large amount of NbNP, as a dry powder (Chapter 4). Developing such technique will make it easy to use these particles in the testing of its catalytic activity with the reported organic reactions (as mentioned, esterification and epoxidation).

1.5 References

1. (a) Smalley, R., In *Congressional Hearings*, 1999;
   (b) Klabunde, K. J., *Nanoscale materials in chemistry*. Wiley-Interscience: New York, 2001; p xi, 292 p.
2. Ludovico Cademartiri, G. A. O., *Concepts of Nanochemistry*. 2009.
3. Ozin, G. A.; Arsenault, A. C.; Royal Society of Chemistry (Great Britain), *Nanochemistry : a chemical approach to nanomaterials*. RSC Pub.: Cambridge, 2005; p xl, 628 p.
4. Schmid, G., *Nanotechnology. Volume 1: Principles and Fundamentals.* . WILEY-VCH: 2008.
5. McGilvray, K. L.; Decan, M. R.; Wang, D.; Scaiano, J. C., *J.A.C.S* **2006,** *128* (50), 15980-1.
6. Steed, J. W.; Atwood, J. L., *Supramolecular chemistry*. 2nd ed.; Wiley: Chichester, UK, 2009; p xxvi, 970 p.
7. (a) Yeom, J.; Wu, Y.; Selby, J. C.; Shannon, M. A., *J Vac Sci Technol* **2005,** *23* (6), 2319-2329;
   (b) Chekurov, N.; Grigoras, K.; Peltonen, A.; Franssila, S.; Tittonen, I., *Nanotechnology* **2009,** *20* (6).
8. Foster, L. E., *Nanotechnology: Science, Inovation and Opportunity*. Prentice Hall: 2005.
9. Astruc, D., *Nanoparticles and catalysis*. Wiley-VCH: Weinheim, 2008; p xxiii, 640 p.
10. Biener, J.; Wittstock, A.; Baumann, T. F.; Weissmuller, J.; Baumer, M.; Hamza, A. V., *Materials* **2009,** *2* (4), 2404-2428.
11. Lopez, N.; Janssens, T. V. W.; Clausen, B. S.; Xu, Y.; Mavrikakis, M.; Bligaard, T.; Norskov, J. K., *J Catal* **2004,** *223* (1), 232-235.
12. Hvolbaek, B.; Janssens, T. V. W.; Clausen, B. S.; Falsig, H.; Christensen, C. H.; Norskov, J. K., *Nano Today* **2007,** *2* (4), 14-18.
13. Huck, W. T. S., *Nanoscale assembly : chemical techniques*. Springer: New York, 2005; p vii, 244 p.
14. Klessinger, M.; Michl, J., *Excited states and photochemistry of organic molecules*. VCH: New York, 1995; p xxiv, 537 p.
15. Turro, N. J.; Ramamurthy, V.; Scaiano, J. C., *Modern molecular photochemistry of organic molecules*. University Science Books: Sausalito, Calif., 2010; p xxxiii, 1084 p.
16. Mayer, J. M., *J Phys Chem Lett* **2011,** *2* (12), 1481-1489.
17. Mayer, J. M.; Barnett, S. M.; Manner, V. W.; Warren, J. J.; Carver, C. T.; Tronic, T. A.; Matson, B. D.; Hayoun, R.; Schrauben, J. N.; Goldberg, K. I., *Abstr Pap Am Chem S* **2011,** *242*.
18. Scaiano, J. C.; Stamplecoskie, K. G.; Hallett-Tapley, G. L., *Chem Commun* **2012,** *48* (40), 4798-4808.
19. McGilvray, K. L.; Fasciani, C.; Bueno-Alejo, C. J.; Schwartz-Narbonne, R.; Scaiano, J. C., *Langmuir* **2012,** *28* (46), 16148-16155.
20. Jockusch, S.; Landis, M. S.; Freiermuth, B.; Turro, N. J., **2001,** *34* (6), 1619-1626.
21. Scherzer, T.; Decker, U., *Vib Spectrosc* **1999,** *19* (2), 385-398.

22. Pacioni, N. L.; Pardoe, A.; McGilvray, K. L.; Chretien, M. N.; Scaiano, J. C., *P.P.S* **2010,** *9* (6), 766-74.
23. Nowak, I.; Ziolek, M., *Chem Rev* **1999,** *99* (12), 3603-3624.
24. Iizuka, T.; Ogasawara, K.; Tanabe, K., *Chem Soc Jpn* **1983,** *56* (10), 2927-2931.
25. Braga, V. S.; Barros, I. C. L.; Garcia, F. A. C.; Dias, S. C. L.; Dias, J. A., *Catal Today* **2008,** *133*, 106-112.
26. Aronne, A.; Turco, M.; Bagnasco, G.; Ramis, G.; Santacesaria, E.; Di Serio, M.; Marenna, E.; Bevilacqua, M.; Cammarano, C.; Fanelli, E., *Appl Catal a-Gen* **2008,** *347* (2), 179-185.

2 • Preparation of Niobium Oxide Nanoparticles: *Mechanistic Investigation*

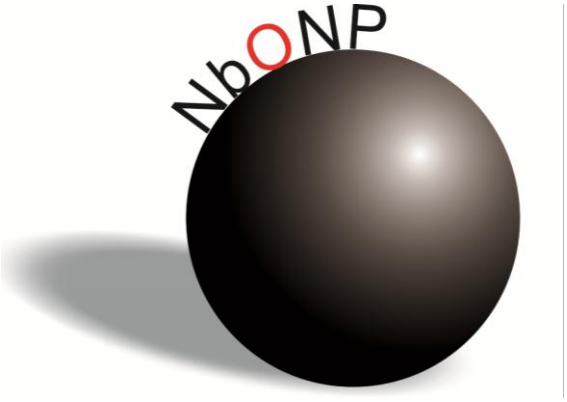

2.1 Photochemical Synthesis of NbNP

As described in the introduction chapter, there are numerous methods in synthesizing metallic nanoparticles. Most of these methods involve chemical reduction of metallic salts by strong reducing agents in the presence of a capping agent that stabilizes the surface of nanoparticles.

The Scaiano group specializes in the preparation of nanoparticles using a photochemical route. This technique is based on the formation of reducing species through UV light irradiation of precursors. As mentioned in Chapter 1, success in the synthesis of Au, Ag and Cu nanoparticles can be achieved using the Irgacures as precursors.[1,2] A variety of Irgacures can be purchased from Ciba Specialty Chemicals (now BASF Global). Upon irradiation with UV light, these compounds generate reducing species by undergoing Norrish type I cleavage. The Irgacure-2959 (I-2959) yields ketyl radicals, whereas Irgacure-907 (I-907) generates α-amino alkyl radicals. I-907 also produces the benzoyl radical, which is thermodynamically less favourable than α-amino alkyl radical that has stronger reducing capabilities (~1.1 V vs. SCE).[3]

Our initial attempts of niobium nanoparticles (NbNP) synthesis showed that I-907 is not just a stronger reducing agent than I-2959, but also yields more monodisperse particles with the minimum amount of aggregation. Thus, we began our studies by designing the optimal conditions for the reactions using I-907 (as will be seen in section **2.1.1**). **Scheme 2.1** shows the reaction sequence in the preparation of NbNP. The photogenerated α-amino alkyl radicals are able to reduce Nb^{5+} to Nb^{4+}. Subsequently, Nb^{4+} then is reduced to Nb^{0} either by a series of α-amino alkyl radicals or through a disproportionation reaction. The Nb^{0} then undergoes

nucleation, followed by seed formation; the growth of which then leads into the formation of NbNP.

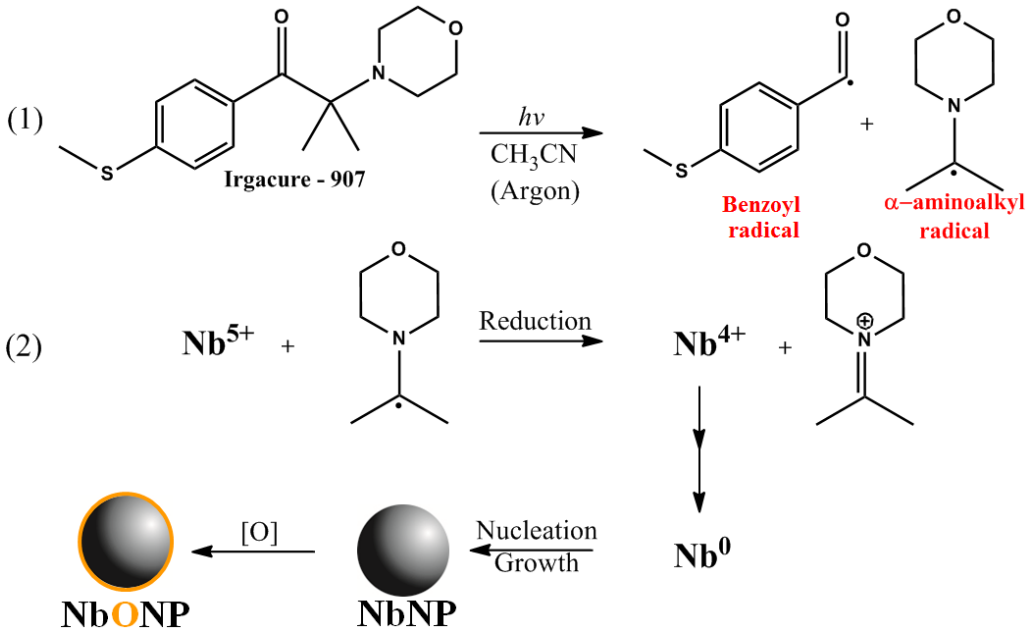

Scheme 2.1 Photochemical sequence into the synthesis of NbNP that leads into the formation of NbONP.

During the formation of NbNP, the process of nucleation and growth using Nb^0 will create metallic particles (NbNP) which oxidize readily upon air exposure to produce stable niobium(V) oxide nanoparticles (NbONPs). The synthesis and the mechanism of formation for NbNP (particles in their un-oxidized form) are described in this chapter. Characterization and properties of NbONPs as a strong Brønsted acid are covered in the next chapter (Chapter 3).

2.1.1 Conditions for Synthesis of NbNP

2.1.2 Irradiation of I-907

While I-2959 is highly soluble in aqueous solutions and has been used in the synthesis of AuNP in water, I-907 is mostly soluble in organic solvents. Synthesis of CuNP using I-907 has been most successful when using acetonitrile as solvent.[2] In initial screening of solvents for synthesis of NbNP, acetonitrile has also demonstrated to be the most suitable as both I-907 and niobium metal precursor are highly soluble in this solvent. In addition, acetonitrile is also inactive towards UVB irradiation. With the wavelength range of 281 - 315 nm, UVB light overlaps with the maximum absorption region of I-907 making it suitable for production of radical pairs from I-907. Therefore, in a control experiment, the solution of I-907 in acetonitrile has been prepared and was irradiated with the UVB light. This process was monitored using absorbance spectroscopy, as seen in **Figure 2.1**.

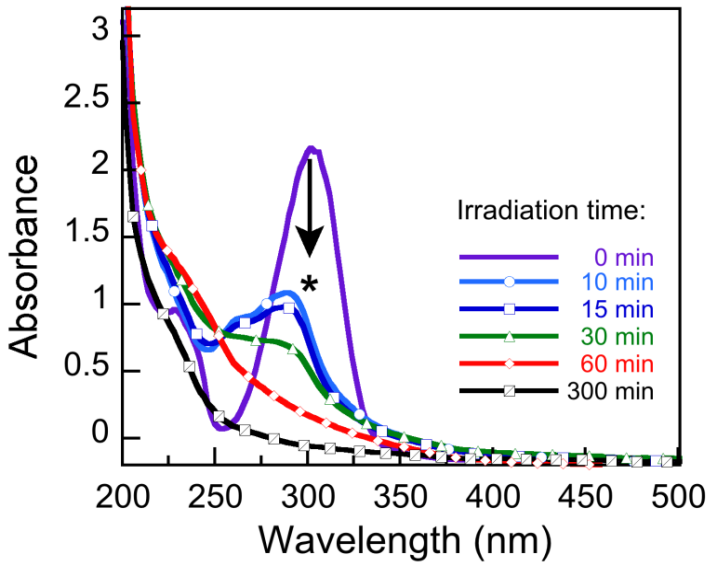

Figure 2.1 Absorbance spectrum of 190 µM solution of I-907 in acetonitrile during photoexcitation with UVB light.[4]

The solution of I-907 (**Figure 2.1**) has been irradiated by the increments of time lengths (10, 15, 30, 60 and 300 minutes) during which the UV-vis absorption has been measured. Prior to its irradiation (0 minutes), I-907 displayed a broad absorbance band at 300 nm. Within the first 10 minutes of irradiation, the I-907 absorbance band has changed into the new band that is blue-shifted relative to the 300 nm band. The absorbance range for the new band (10 minutes) is from 250 nm to 320 nm. Thus, we can conclude that, within the first 10 minutes of irradiation, I-907 undergoes photochemical dissociation into its related photoactive by-product (this was confirmed with GC-MS analysis, section 2.3). Furthermore, the absorbance (*) of this photoactive by-product also falls within the UVB range, and therefore becomes susceptible to the irradiation. After 300 minutes of further irradiation, the sample undergoes complete photobleaching, as seen in **Figure 2.1**.

Results of this experiment have established that the maximum time needed for I-907 irradiation and its related photoactive by-product is 300 minutes. After 300 minutes of irradiation, the sample does not contain UVB photoactive compounds.

Note:

All irradiation experiments except the large scale synthesis using the 100 mL quartz tube (for experimental details, see **Chapter 4**) were performed inside a Luzchem photoreactor equipped with 14 UVB bulbs (62 W/m^2). Furthermore, samples were under constant rotation inside the photoreactor to allow equal irradiation.

2.1.3 Niobium precursor

Initial niobium precursors selected for the synthesis of NbNP were niobium(V) chloride ($NbCl_5$) and niobium(V) ethoxide ($Nb(OCH_2CH_3)_5$). Both of these precursors were found to be easily susceptible to hydrolysis. The addition of these precursors into "wet" acetonitrile resulted in white precipitate. As a result, in the follow-up experiments, acetonitrile was cleaned using the purification system (LC Technologies, details in Section 2.6). The resulted dry acetonitrile was now suitable for preparation of stock solutions of Nb(V) precursors.

Under dry conditions, each of the precursors was used to generate NbNP using I-907 as a photoinitiator. The TEM analysis of the generated particles demonstrated low reaction yields, as well as poor monodispersity of these particles. Out of the two precursors, reactions with $NbCl_5$ were with lowest yields, and therefore, this Nb(V) precursor was not used in further experiments.

To obtain improved results in the synthesis of NbNP, it was necessary to modify $Nb(OCH_2CH_3)_5$ by substituting the ethoxide ligands with acetylacetone (Hacac). Such modification was inspired from the works of Sortino *et al.* who used Ag(acac) as a precursor for the AgNP synthesis.[5] Their work demonstrated that acac, as a coordinated ligand, can be displaced from the complex with the metal ion; thus easing the process for reduction of the metal ion and leading to growth of nanoparticles. To test this approach, a reaction method for the synthesis of $Nb(acac)_5$ was developed (experimental details at Section 2.6).

The preparation method of $Nb(acac)_5$ involves a stoichiometric ligand exchange of ethoxide in $Nb(OCH_2CH_3)_5$ with Hacac to generate $Nb(acac)_5$ and ethanol. Since $Nb(OCH_2CH_3)_5$ is susceptible to hydrolysis, this reaction was completed under dry conditions.

To maintain these conditions and to avoid exposure to air, Raman spectroscopy was used as technique to follow the reaction's progress (results are illustrated in **Figure 2.2** below).

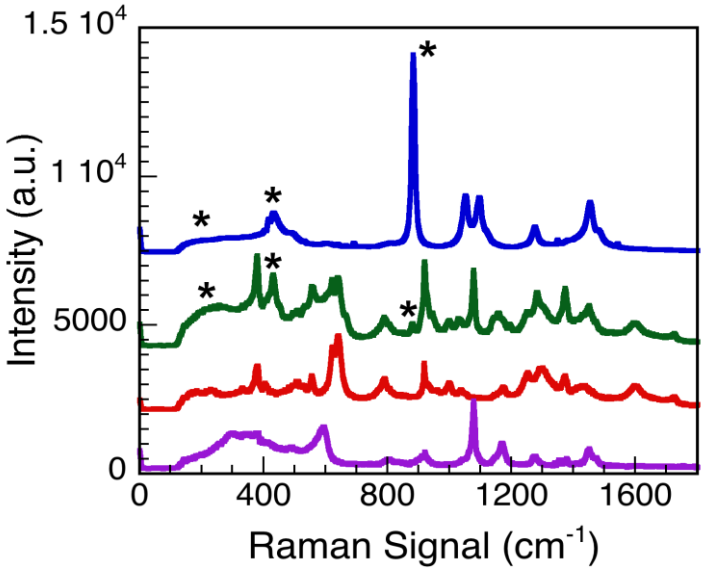

Figure 2.2 Raman spectra of ethanol (—), $Nb(acac)_5$ in acetonitrile (—), acetylacetone in acetonitrile (—) and $Nb(OCH_2CH_3)_5$ in acetonitrile (—).[4]

Inorganic complexes, such as $Nb(OCH_2CH_3)_5$, are easier to analyze by Raman spectroscopy than by other spectroscopic methods, such as infrared spectroscopy. Raman spectra are acquired quickly and contain highly specific spectral fingerprint for a compound. In **Figure 2.2**, the Raman spectra of $Nb(OCH_2CH_3)_5$ and Hacac demonstrated distinctive characteristics (bands at 600, 920, 1080, 1160, 1275, 1450 cm^{-1} for $Nb(OCH_2CH_3)_5$ and bands at 400, 570, 650, 800, 1600 cm^{-1} for Hacac). After the reaction of these compounds with one another, a new set of bands emerged, due to formation of $Nb(acac)_5$. The bands denoted by the asterisk (*) are of specific interest. These bands correspond to ethanol, thus acting as confirmation for successful release of ethoxide from $Nb(OCH_2CH_3)_5$ in generation of $Nb(acac)_5$.

After the confirmation from the Raman spectroscopy experiments, $Nb(acac)_5$ was then used as a niobium precursor together with I-907 to generate NbNP. This precursor was used to generate particles in high yields and with excellent monodispersity, as confirmed by TEM (Section 2.1.5). The success with using $Nb(acac)_5$ led us to employ it in the synthesis of NbNP in this thesis.

Although Raman spectrometry provided confirmation that the release of ethoxide happened, it gives no insight to how many of acac ligands are bound to Nb^{5+} and what is the coordination geometry of the niobium in this complex. Since the acac ligand can be mono- and bi-dentate and the coordination number for the central atom is likely to be 6 or 7, it is clear that some ligands in $Nb(acac)_x$ will be coordinated in the monodentate fashion and some ligands will be coordinated in the bidentate fashion. Work performed by Sedlar and co-workers demonstrated that in the substitution of $Nb(OCH_2CH_3)_5$ with a single Hacac, the product $Nb(OCH_2CH_3)_4(acac)$ proved to be monomeric with a symmetrically bound acac group.[6] Unfortunately, to the best of author's knowledge there was no further literature reports on the structure of $Nb(acac)_x$. Therefore, the formation of $Nb(acac)_5$ is in assumption that acac is coordinated in the monodentate fashion and is work for a future studies.

Note: No formation of NbNP was observed when the UVB irradiation of $Nb(acac)_5$ solution performed without I-907. The addition of acetylacetone to the $Nb(OCH_2CH_3)_5$ solution with I-907 prior to its irradiation resulted in NbNP with low yields and monodispersity. This experiment demonstrated that acetylacetone does not play a role in the growth of NbNP, but is important as a ligand in $Nb(acac)_5$ that aids in the generation of particles.

2.1.4 Air Sensitivity

It was detected in the original synthesis that, if the reaction quartz cuvettes (7mm x 7 mm) or other related stock solution flasks were not properly purged with inert gas, aggregation and incomplete particle formation occurred. Additionally, the growth of nanoparticles is quenched if they are exposed to air. Thus, industrial T (99.9%) argon gas was used in preparation of all stock solutions and for purging quartz cuvettes before irradiations (details described in Experimental Section).

2.1.5 Time of Irradiation

Various factors influence the growth and monodispersity of nanoparticles. By standardizing irradiation conditions, such as choosing specific wavelength and timing, we define experimental conditions and eliminate the possibility for random dispersion. After standardizing UVB lamps as the source of specific wavelength range, we performed an experiment to determine the timing for its irradiation. We irradiated the solution of I-907 (190 µM) and $Nb(acac)_5$ (10 µM) for defined periods of time (10, 15, 30, 60 and 300 minutes), during which the UV-Vis absorbance (**Figure 2.3**) was measured, and the probes were taken for TEM analysis (**Figure 2.4)**.

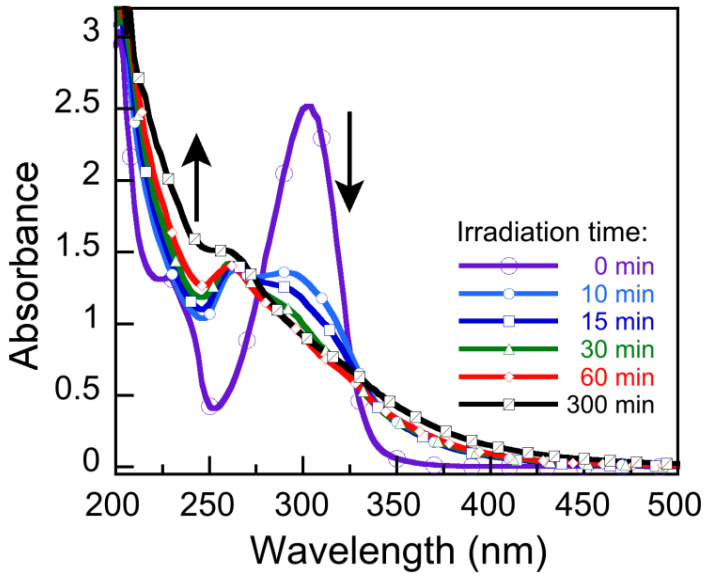

Figure 2.3 Absorption spectra during UVB irradiation of I-907 (190 µM) and $Nb(acac)_5$ (10 µM) in acetonitrile.[4]

Figure 2.3 shows absorption spectra during the UVB irradiation of the $Nb(acac)_5$ / I-907 mixture. The particle formation can be seen via the scatter plot at the final reading time (Note: the location and difference of the (—) curve for 300 minutes vs. its locations in **Figure 2.1** during the simple I-907 photodecomposition). Although the scatter plot is an indication of NbNP formation, it provides no extra information on the size and morphology of these nanostructures. A small droplet from the sealed sample was extracted via a needle syringe (to prevent any unwanted oxidation) for TEM analysis.

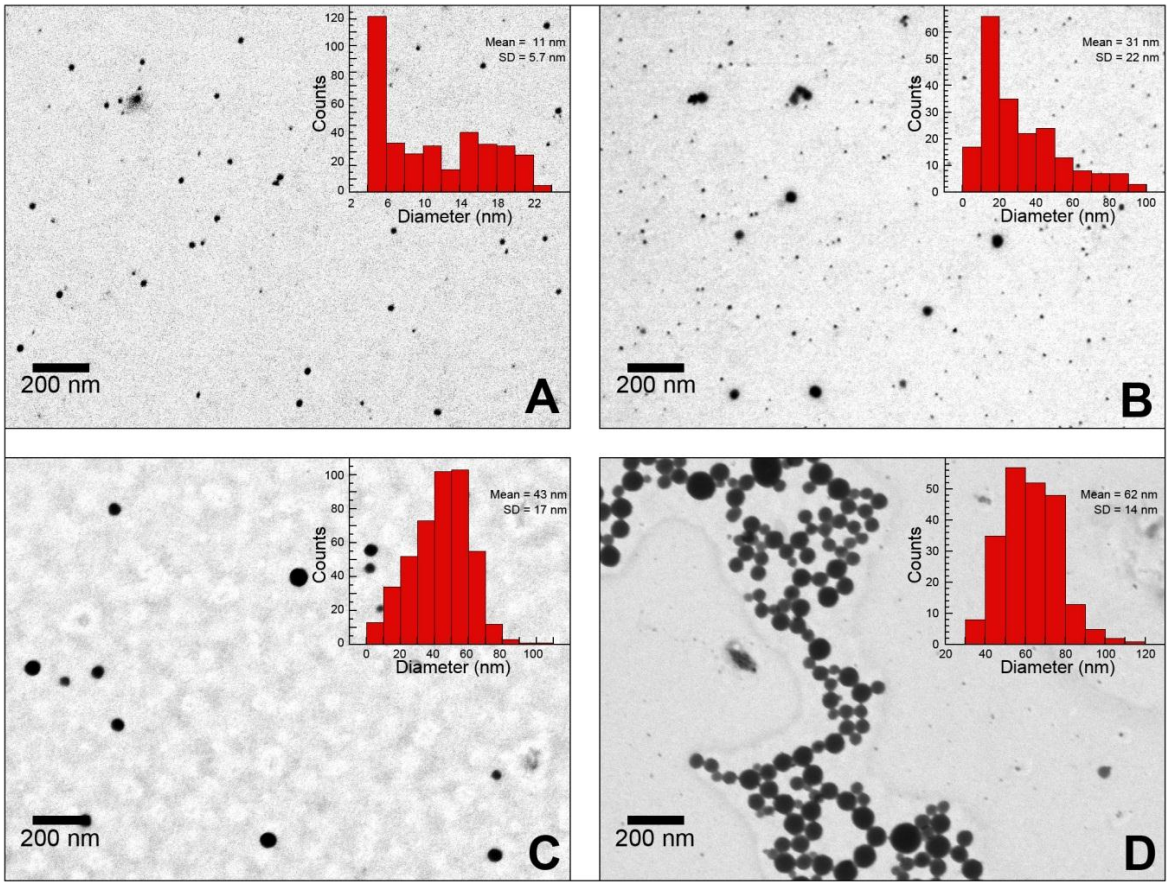

Figure 2.4 Formation of NbNP after 10 minutes (A), 30 minutes (B), 60 minutes (C) and 300 minutes (D) of UVB irradiation as examined by TEM.[4]

In **Figure 2.4,** the TEM images illustrate that the size of particles increased during the 300 minutes of irradiation. This size increase is of ~6x enlargement, as seen from the period of 10 minutes of growth (the mean size of 11 nm) to the final 300 minutes (the mean size of 62 nm, see **Figure 2.5)**.

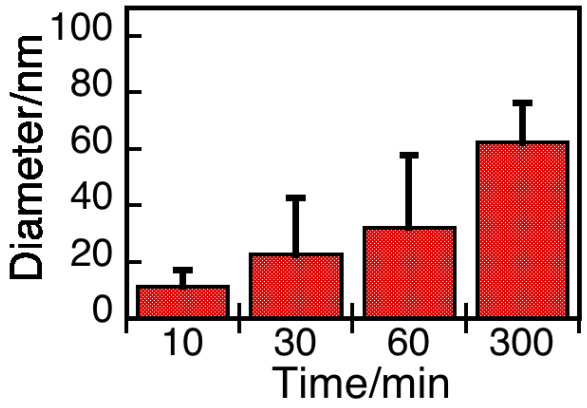

Figure 2.5 Enlargement of NbNP diameter during photoirradiation. NbNP sizes were calculated using a mean of 100 individual nanoparticles.[4]

Irradiation of the sample after 300 minutes provided no further change to the final size of particles. Consequently, 300 minutes was the maximum time of irradiation for all samples, except for when using the 100 mL quartz cuvette for preparation of NbNP for XPS.

2.1.6 Effect of Irradiation on the growth of NbNP

Since the decomposition of I-907 occurs within the first 10 minutes of irradiation, one may assume that continuous growth of NbNP may be independent from further irradiation. Therefore, the need for I-907 to generate radicals for rapid nucleation (seeds formation) is established, but the follow up for growth steps should occur spontaneously on their own. In the following control experiment the solution of I-907 (190 µM) and $Nb(acac)_5$ (10 µM) was irradiated for 10 minutes and then kept in the dark for 300 minutes. The experiment was monitored using UV-Vis and TEM. **Figure 2.6** below shows the results for UV-vis absorbance.

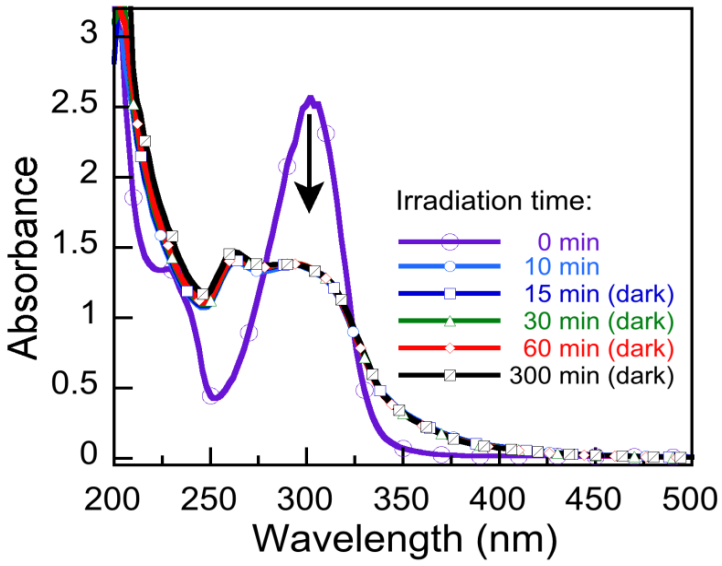

Figure 2.6 Absorbance of 190 µM I-907 and 10 µM $Nb(acac)_5$ in acetonitrile after UVB irradiation for 10 minutes, followed up by placing the sample in the dark until 300 minutes.[4]

From **Figure 2.6**, we observed that within 10 minutes all of I-907 was photo-decomposed into its photoproducts, which are not susceptible to any further photobleaching due to the lack of UVB irradiation, as compared to the results in **Figure 2.1**. Correspondingly, throughout the 300 minutes we did not see any scatter formation that was associated with the growth of NbNP, as it was noted before (**Figure 2.3)**. In fact, the TEM results for this experiment demonstrated formation of only tiny particle seeds with a ~10 nm mean size, exactly like the ones seen in **Figure 2.4 (A)**. Such results support the idea that initial nucleation occurs within the first 10 minutes, but contradict the notion that NbNP may grow without further UVB irradiation.

2.1.7 Summary of conditions for synthesis of NbNP

It has been demonstrated that by varying the wavelength and time of irradiation, changes to the shape of nanoparticles occur. For instance, in the synthesis of AgNP: irradiation of $AgNO_3$ with I-2959 in water for 30 minutes using 405 nm wavelength results into the formation of spherical nanoparticles, whereas irradiation of the same solution using 455 nm for 3 hours results into particles with decahedral shapes.[7] In this study, we focused on maintaining the same length of irradiation and the excitation wavelength for all of the experiments. Consequently, the notion of using various wavelengths to change the particle shape was ruled out as an option.

In these experiments, we have established that the growth of NbNP is continuous until 300 minutes of UVB irradiation. Stopping irradiation after 10 minutes and then keeping the samples in the dark had prevented further growth of NbNP. This suggests that after 10 minutes of UVB irradiation (coincident with complete I-907decomposition), any further changes in the growth of NbNP are strongly linked to the photoactivity of an I-907 photoproduct.

2.2 Controlling the size of NbNP

Under the established conditions, we performed an experiment to test if the concentration of I-907 affects the size of NbNP. When the concentration of I-907 was increased from 60 to 730 µM while keeping the same $Nb(acac)_5$ concentration (10 µM), the size of NbNP produced increased from 10.4 ± 4.4 nm to 86 ± 50 nm (**Figure 2.7**).

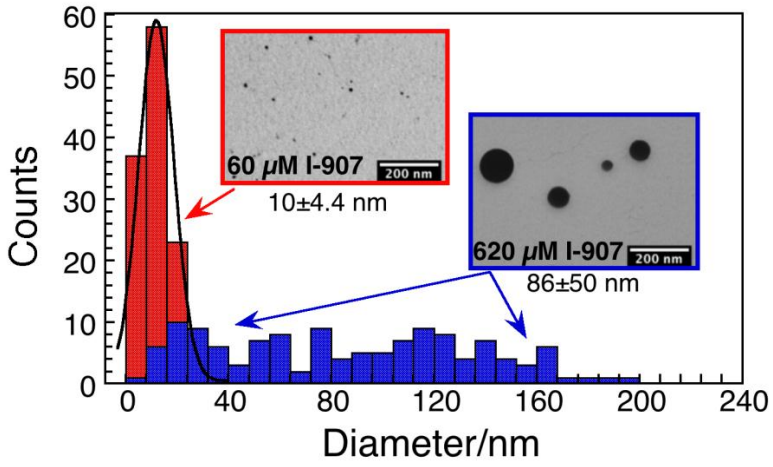

Figure 2.7 Size distribution of two NbNP samples obtained from solutions with 60 µM (red) and 620 µM (blue) concentrations of I-907. Insets depict TEM images of the samples.[4]

Accordingly, the size of NbNP is dependent on the concentration of I-907. We confirmed this dependency by completing a series of reactions where the concentration of $Nb(acac)_5$ was kept constant (10 µM) and the concentration of I-907 varied from 60 µM to 730 µM (**Figure 2.8)**.

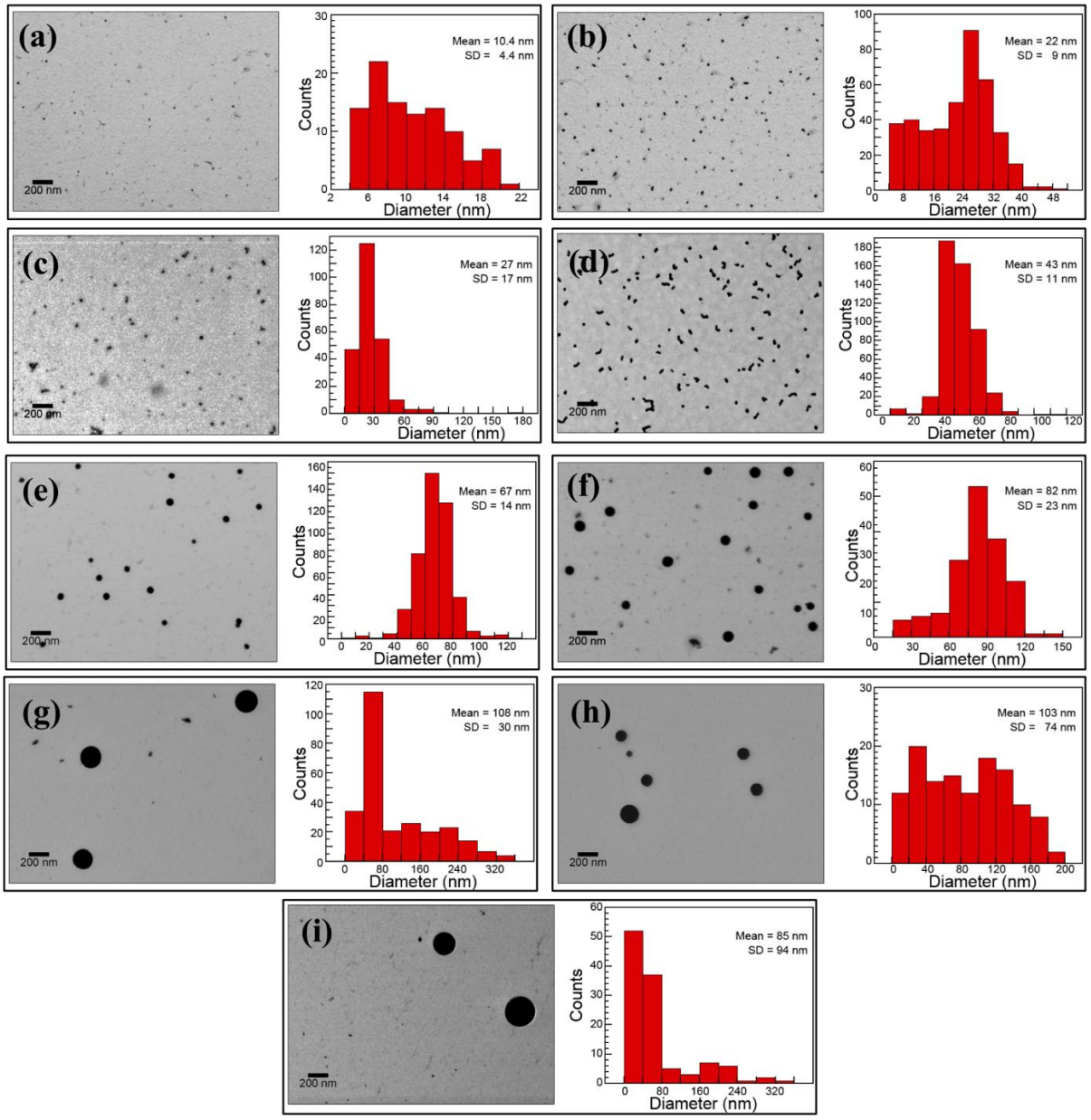

Figure 2.8 TEM analysis (left) and its related size distribution histograms (right) of NbNP prepared from solutions with 10 µM $Nb(acac)_5$ and (a) 60 µM, (b) 80 µM, (c) 100 µM, (d) 190 µM, (e) 260 µM, (f) 420 µM, (g) 520 µM, (h) 620 µM and (i) 730 µM I-907.[4] The size bar corresponds to 200 nm in each of TEM images.

Figure 2.8 combines TEM analysis (image of NbNP and its related size distribution histogram) for samples of particles that been generated with varying I-907 concentrations. As seen from TEM images, the increase in size is proportional to the amount of I-907 added. Correspondingly, the data collected had demonstrated a positive correlation trend between the mean diameter of NbNP and its related increase of I-907 concentration, as may be seen in **Figure 2.9**.

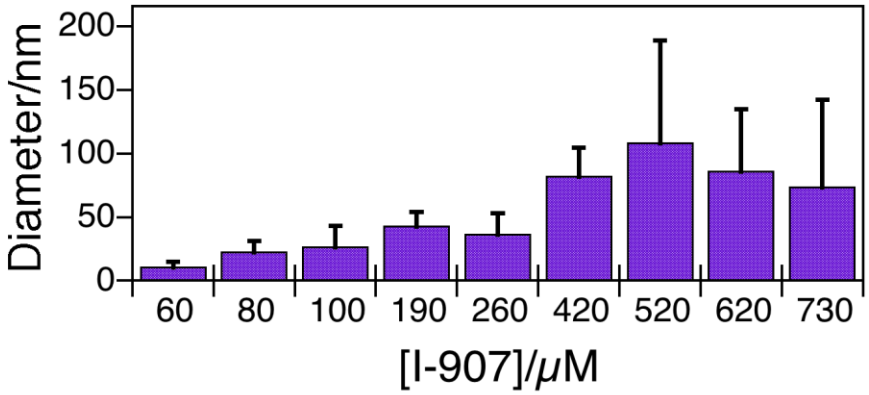

Figure 2.9 NbNP mean diameters obtained after 300 minutes irradiation of solutions containing 10 μM $Nb(acac)_5$ and varying concentrations of I-907. NbNP sizes were calculated from an average of at least of 100 individual nanoparticles.[4]

As additions of reducing agent are increased, into the solution with metal precursor, this will result into the formation of smaller particles (Chapter 1). Previous experiments confirmed this observation during the synthesis of AuNP using a photochemical approach.[8] As the amount of I-2959 photoinitiator was increased at a fixed Au(III) concentration, the size of AuNP decreased. However, an opposite effect was observed in the synthesis of NbNP, where increasing

concentration of I-907 increased particles mean diameter (**Figure 2.9).** Nevertheless, this effect reaches its limits at 520 µM, whereas an increase in concentration of I-907 at 620 µM and 730 µM demonstrates a decrease in NbNP mean size due to the broadening in dispersity of its size.

Photochemically generated AgNP and AuNP can have unprotected surfaces, thus providing opportunity for their further growth via seed-mediated processes.[8-9] Addition of metal salts and mild reducing agents to these photogenerated particles results into the further growth of these nanoparticles.[10] In this process, only *mild* reducing agents are used, such as ascorbic acid for AgNP or hydroxylamine hydrochloride for AuNP, so that generation of new seeds which may lead to the formation of smaller sized particles is prevented.[11] Therefore, the mechanism of growth of these particles is dependent on how ligand-free their surfaces are, for they become active sites for deposition of new atom layers that are reduced by mild agents.[12]

The synthesized NbNP do not contain any additional surfactants during their synthesis. Thus, these particles contain largely unprotected surfaces that are suitable for further growth, as was observed with the photogenerated AgNP and AuNP.[11] Henceforth, the growth of NbNP may also be guided via a seed-mediated mechanism. Consequently, this may explain the reason for the size increase trend that was observed in **Figure 2.9**. When solutions with an increased concentration of I-907 were irradiated, higher concentrations of I-907 side products were generated. Therefore, if these side products are capable of acting as mild reducing agents, they can support continuous growth of NbNP over 300 minutes and, thus, the mechanism of seed-mediated growth can be at play.

2.3 Investigation of I-907 Photoproducts

We have established that a solution of I-907 after 10 minutes of UVB irradiation undergoes a complete photodecomposition into its related photoproducts (**Figure 2.1**). Specifically, one of the photoproducts, just like I-907, is also able to absorb a light at 300 nm in the UV-Vis spectrum. To further investigate the structure of that product and other photoproducts, the GC analysis of an I-907 reaction mixture was performed (**Figure 2.10)**.

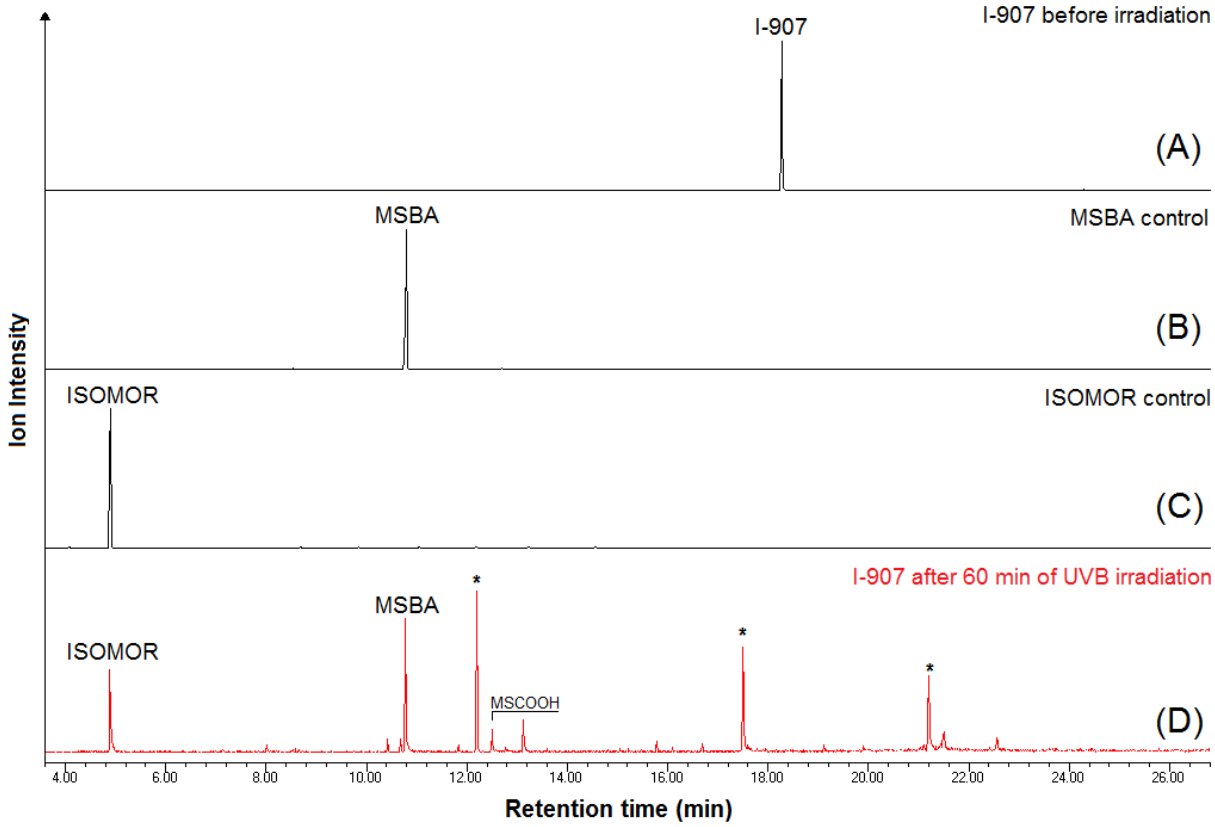

Figure 2.10 GC analysis of (A) 190 µM I-907, (B) 190 µM MSBA, (C) 190 µM isopropylmorpholine and (D) a solution of 190 µM I-907 after 60 minutes of UVB irradiation (in CH_3CN solution and under argon).[4]

Note: * denote the formation of secondary photoproducts.

The GC analysis showed the formation of two major I-907 photoproducts: 4-(methylthio)benzaldehyde (MSBA) and 4-N-isopropylmorpholine (ISOMOR) (**Figure 2.11)**. Purchased sample of MSBA and synthetically prepared ISOMOR were used as controls to verify their identities as the major I-907 photoproducts.

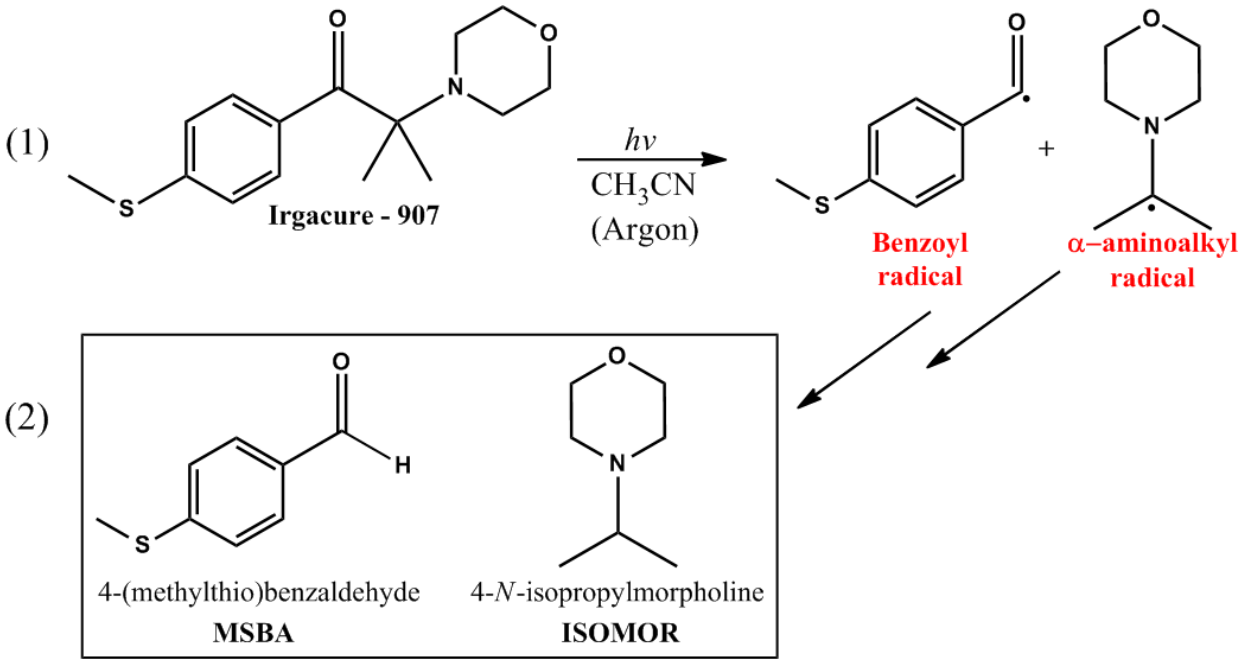

Figure 2.11 (1) Photodecomposition of I-907 into two types of radicals (2) Major photoproducts of I-907 irradiation: MSBA and ISOMOR.

Upon irradiation, I-907 acts as a photoinitiator of both benzoyl and α-aminoalkyl radicals. However, the synthesis of NbNP only depends on the formation of α-aminoalkyl radicals and their ability to act as strong reducing agents for $Nb(acac)_5$ (**Scheme 2.1**). Whereas the unused benzoyl radicals did not perform well as reducing agents and instead became an available precursor for the generation of MSBA.

Similar to our findings, Turro *et al.* reported the formation of MSBA as a product generated from the benzoyl radical.[13] In their GC study, MSBA was also found to be a major by-product of 2-hydroxy-1,2-bis-(4-methylsulfanyl-phenyl)-ethanone (MTB) photodecomposition, as seen in **Figure 2.12**.

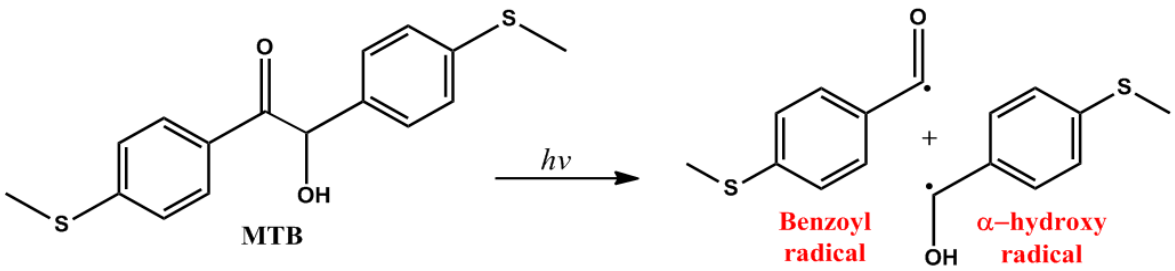

Figure 2.12 Photodecomposition of MTB into two types of radicals: Benzoyl and α-hydroxy radicals. While α-hydroxy radical acts like an excellent reducing agent in polymerization, the benzoyl radical spontaneously forms into MSBA.[13]

Turro *et al.* explained the formation of the MSBA photoproduct by H-abstraction of the benzoyl radical from available H-donors.[13] In agreement with their findings, we rationalize that the formation of MSBA from I-907 is also the product of such disproportionation reaction. Furthermore, solvent of our choice (acetonitrile) is likely contaminated with traces of water that can act as indirect source for the protons. The confirmation for the presence of water is the formation of 4-(methylthio)benzoic acid (MSCOOH) that was found in the GC analysis. Secondary photoproducts of I-907 (denoted as* in **Figure 2.10**) were also found. These minor products are dimers formed due to the radical recombination, such as benzoyl derivative (benzoyl radical + benzoyl radical) or ISOMOR derivative (α-aminoalkyl radical + α-aminoalkyl radical).

2.4 MSBA and its Effects on the Growth of NbNP

The investigation of I-907 photodecomposition demonstrated MSBA and ISOMOR as the major by-products after irradiation (Section 2.3). Purchased sample of MSBA and synthetically prepared ISOMOR were used to further determine their roles in the growth of NbNP. **Figure 2.13** represents the change in size of NbNP due to the addition of 560 µM ISOMOR or MSBA after 5 minutes of UVB irradiation of solution containing 60 µM I-907 and 10 µM $Nb(acac)_5$. Following those additions, after 5 minutes the samples were further irradiated for the total of 300 minutes.

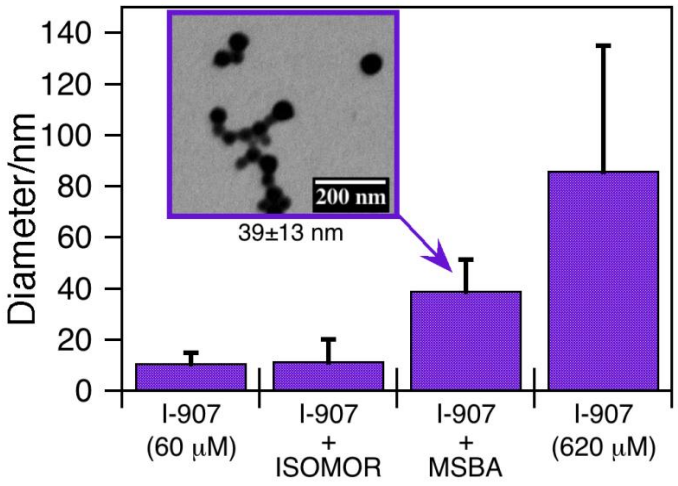

Figure 2.13 Variation in NbNP mean size for samples with 10 µM $Nb(acac)_5$ and 60 µM I-907 that had been UVB irradiated for 5 minutes and followed by the addition of 560 µM MSBA or ISOMOR. The data of 620 µM I-907 was included for size comparison. T-test statistical analysis demonstrated the statistical data difference ($p < 0.001$) in all of the cases.[4]

We observed that at the fixed 60 µM concentration of I-907, the maximum size that particles could reach after 300 minutes of irradiation were 10 ± 4.4 nm in diameter (**Figure 2.13**). An addition of 560 µM ISOMOR to a sample containing 60 µM concentration of I-907 caused no significant changes to the size of NbNP. However, the addition of 560 µM MSBA caused an increase in the size of NbNP by a factor of 4, up to the size of 39 ± 13 nm in diameter when compared to the control. This suggests the involvement of this I-907 photoproduct in the growth in NbNP. Hence, if MSBA is indeed capable to act as a mildly reducing agent, then it is possible to use it directly with $Nb(acac)_5$ for the synthesis of NbNP. The attempted experiment of such a proposition was very successful, as can be seen from the UV-Vis spectra in **Figure 2.14**.

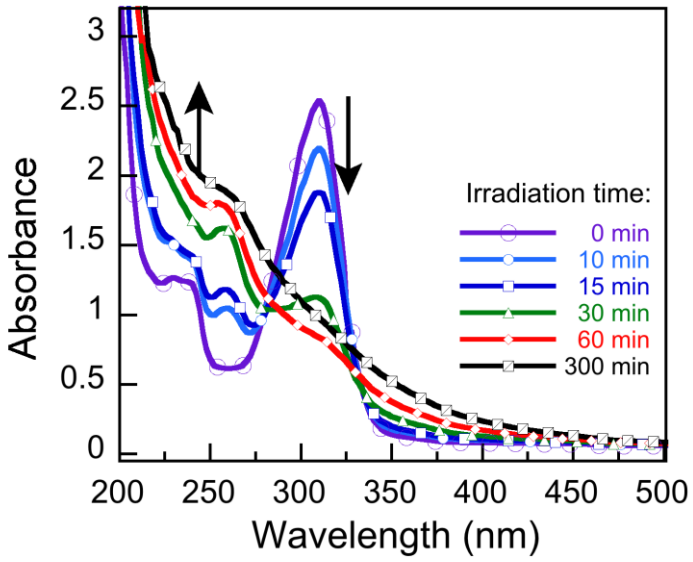

Figure 2.14 UVB irradiation of 190 µM MSBA and 10 µM Nb(acac)5 in CH_3CN under argon.[4]

During 300 minutes of MSBA irradiation, MSBA undergoes photobleaching simultaneously with growth of NbNP as illustrated by the increased scattering at ~230 nm (**Figure 2.14**). In addition, the MSBA absorbance band in the UV-Vis absorption spectrum (**Figure 2.14)** matches the absorbance band that was formed after 10 minutes of I-907 irradiation (**Figure 2.3)**. This confirms the GC results: it is MSBA that is being formed and acting as a primarily complex for absorbance of the UVB light in the synthesis of NbNP.

We were able to reproduce the trend of the nanoparticle size increase due to I-907 concentration, but this time substituting I-907 with MSBA as the only source of reducing agent (**Figure 2.9**). The results for UVB irradiation of solutions containing 10 μM $Nb(acac)_5$ and varying concentrations of MSBA are shown in **Figure 2.15**.

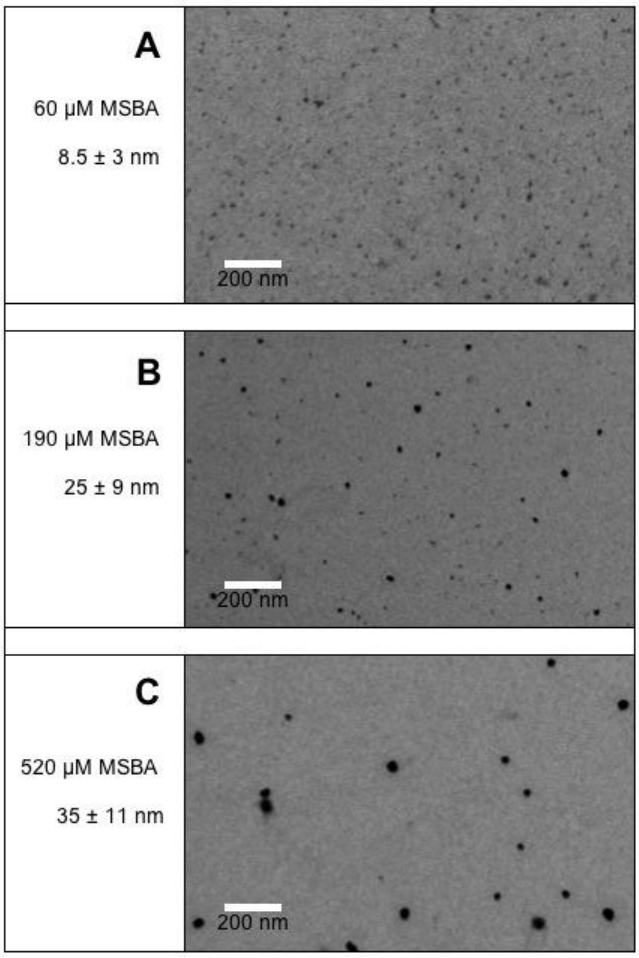

Figure 2.15 Represents TEM images of samples containing 10 µM $Nb(acac)_5$ and (A) 60 µM, (B) 190 µM and (C) 520 µM MSBA. From the average sizes (represented to the left of each image), it was found that the diameter of NbNP increased correspondingly with the MSBA concentration increase.[4]

2.5 Mechanism of the Growth of NbNP

2.5.1 The role of MSBA

The results from MSBA experiments (illustrated in **Figure 2.15)** without a doubt exhibited the similar trend that we have observed when using the concentration of I-907 to control the size of generated NbNP. This strongly suggests the involvement of MSBA in light-mediated mechanism of NbNP synthesis. To gain further insight into the activity of MSBA, a GC-MS analysis was performed with a solution of 190 µM MSBA, as seen in **Figure 2.16**

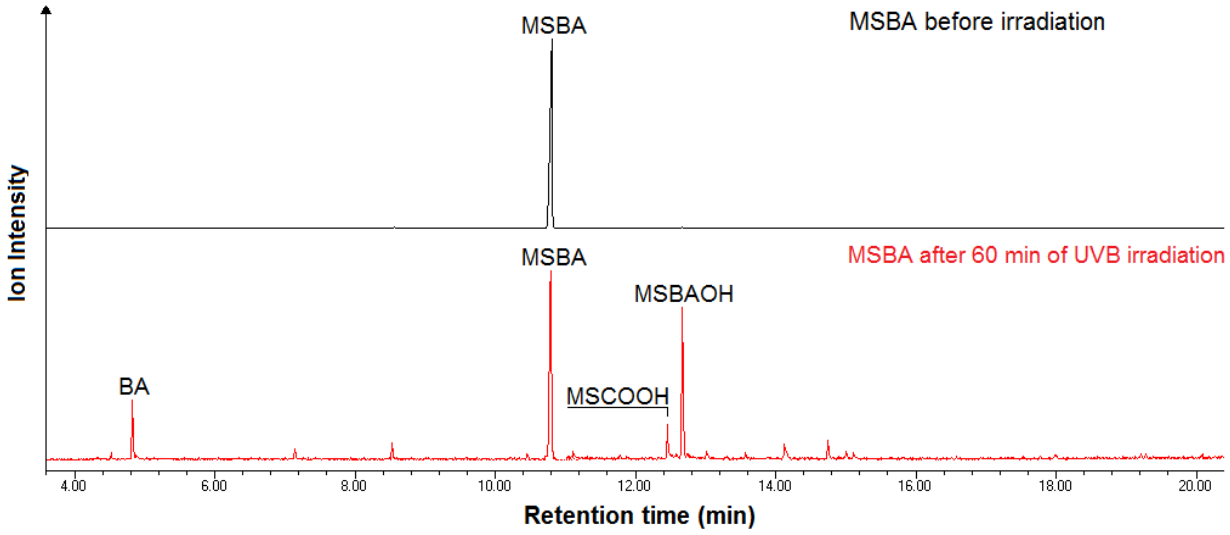

Figure 2.16 GC analysis of 190 µM MSBA after 60 minutes of UBV irradiation (all performed in CH_3CN and under argon). (MS results for this GC analysis are displayed in Appendix 2.7)

From the results of the GC-MS analysis, we were able to identify three major products from the UVB irradiation of MSBA: benzaldehyde (**BA**), hydroxy-4-(methylthio)benzaldehyde (**MSBOH**) and 4-(methylthio)benzoic acid (**MSCOOH**). The formation of these molecules signifies that an important photochemical pathway must have occurred in order for those molecules to have been formed, **Scheme 2.2**.

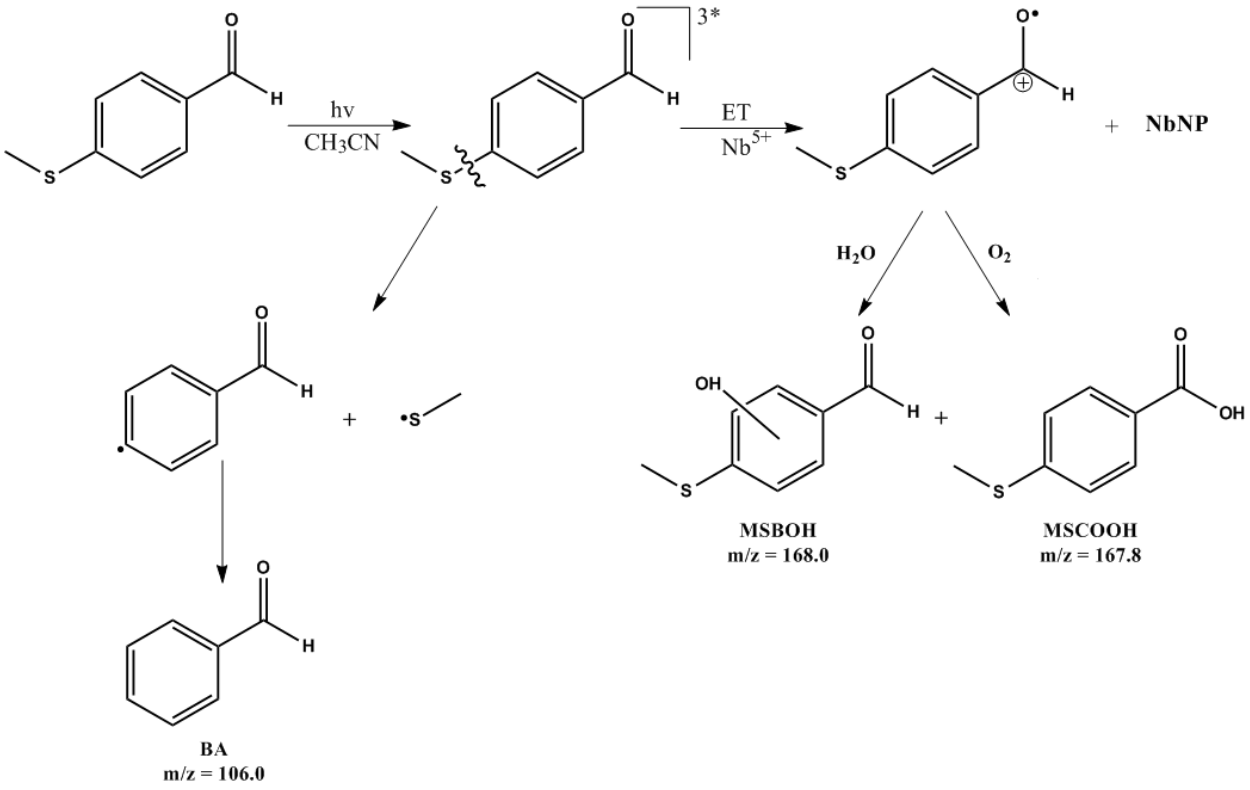

Scheme 2.2 Illustrates a formation of reported photoproducts from UVB irradiation of MSBA in solution of CH_3CN under argon. Note: the solvent CH_3CN is contaminated with the traces of water. Formation of MSCOOH is most likely due to the traces of O_2, hence the smallest intensity for the GC peak.

The proposed **Scheme 2.2** depicts that MSBA, upon its irradiation with the light, gets excited into its triplet state (^{3}MSBA). Once in an excited state, an electron transfer may take place to remove an electron from ^{3}MSBA to Nb^{5+} atom (or into niobium surrounding ligand: acetylacetone). The niobium atoms are then reduced to form seeds, which can then grow into large NbNP from the reduction of more niobium ions into their surface. Equally, this pathway results in formation of MSBA into its cationic radical intermediate that may react with the traces of water generate MSBOH or with oxygen to generate MSCOOH.

The mechanism for the formation of NbNP using ^{3}MSBA as an active reducing agent is supported by similar studies that had been done previously, but using benzophenone as absorbing chromophore. The irradiation of benzophenone activates via the hydrogen abstraction into the formation of a ketyl radical.[14] Accordingly, this ketyl radical is then capable of acting as a reducing agent in the presence of silver ions leading them into the formation of AgNP.[15] In our lab, we further utilized this method for the synthesis of AuNP using benzophenone and $HAuCl_4 \cdot 3H_2O$.[16] Significantly, the reduced rates of AuNP formation had been noted when using benzophenone under aerobic conditions.[16] Such decrease in the rates is attributed to the triplet being quenched by oxygen. Due to the oxygen rate constant approaching diffusion-controlled values, NbNP seizes growth instantly upon air exposure.

In the final analysis of **Scheme 2.2**, we noted the formation of a BA compound, the generation of which must require MSBA to undergo a C-S bond cleavage. In fact, studies by Marciniak *et al* reported that the photochemical cleavage of C-S bond in the 4-(methylthio)phenylacetic acid may only occur exclusively via a triplet-state activation (Φ = 0.17).[17] That is, even though their compound is slightly structurally different from MSBA, it may

still provide a positive support to the possibility of MSBA to generate $\cdot SCH_3$ radicals via photoactivation.

To summarize, it is difficult to conclusively state which of the two MSBA mechanistic pathways dominates in the reduction of Nb^{5+} ions. The performed MSBA experiments provide an insight into the possibilities for both of these pathways to actively act in formation of NbNP, but any more detail on their quantum yield; for that a further study will be necessary.

2.5.2 Mechanism of NbNP growth using I-907

The proposed mechanism for the formation and growth of NbNP is shown in **Scheme 2.3**. We can describe this mechanism by the series of events: (1) irradiation of I-907 generates a pair of radicals (α-amino alkyl and benzoyl), (2) each of these radicals undergoes its own specific reaction to produce products, such as: (i) MSBA from the benzoyl radical and (ii) NbNP seeds from the α-amino radical. Finally (iii), the generated seeds then undergo further growth via irradiation of MSBA that acts as a mild reducing agent.

The proposed mechanism follows a seed-mediated synthesis where each of its components is in symbiosis to achieve the final growth of NbNP. However, this mechanism provided no insight in explaining the trend for the size increase of particles with an increase in MSBA concentration. The explanation to this phenomenon is suggested here, in this final section.

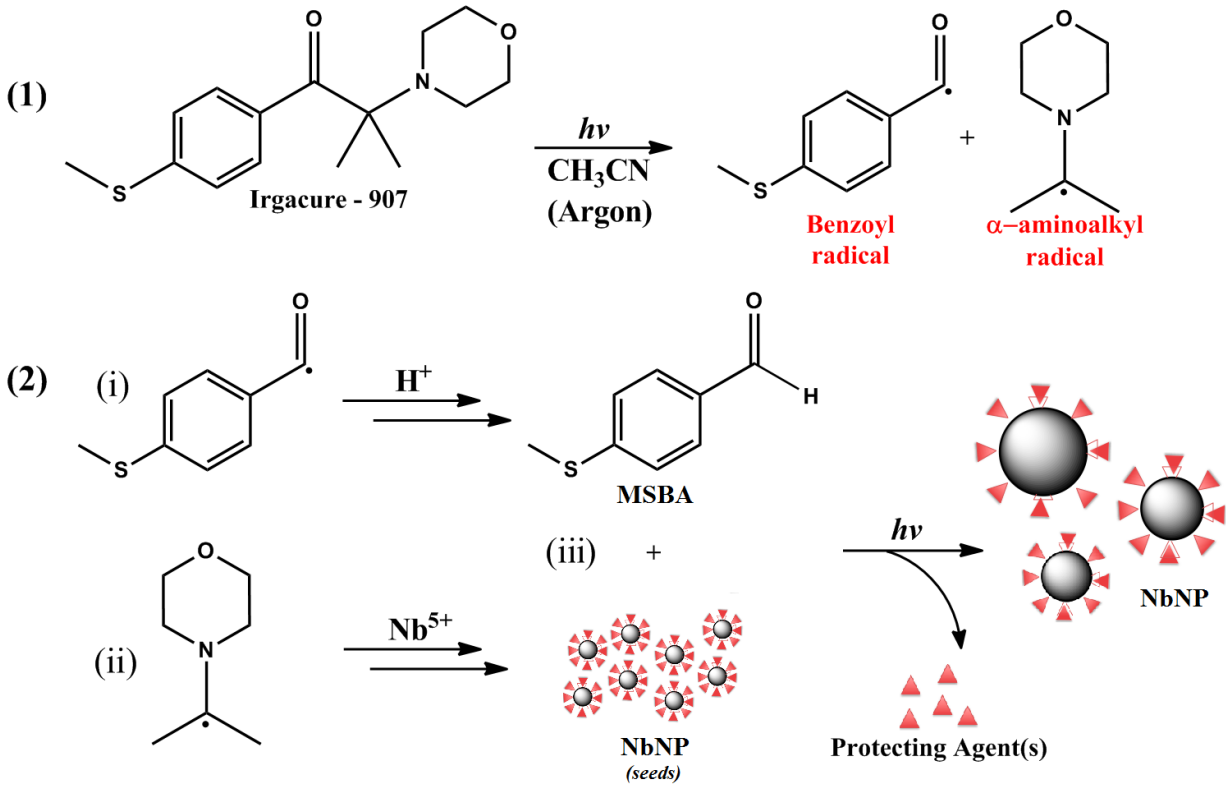

Scheme 2.3 Proposed mechanism for the growth of photochemically generated NbNP.

In the studies by Murray *et al.* for the synthesis of size controlled AuNP, the authors were able to establish an emerging trend; that the increase in the diameter of the gold particle must correspond to the decrease in percentage of organic stabilizers on its surface.[18] Accordingly, the decrease of organic stabilizers correlate to the lower packing density on the surface of gold atoms, thus exposing them to further bind with metal ions.[18]

Following this notion, Workentin *et al.* reported that the photochemical generation of acyl and tert-butyl radicals (from irradiation of pivalophenone **2** (**Table 1** of Chapter 1)), in the presence of alkylthiolate-modified AuNP, causes binding of these radicals with the sulfur atom of these alkylthiolates.[19] Such changes in the surfactants causes decrease in their interaction with

the surfaces of AuNP, consequently releasing them from the surfaces and permitting the further growth of AuNP.[19]

In summary, aside from MSBA being the source for further Nb^{5+} reductions, it can also act as a promoter for abstraction and replacement of the surfactants surrounding NbNP. Upon increased concentration, MSBA intervened with the protective ligands of NbNP, releasing them and exposing the metallic surface, which in turn caused particles' further growth. The proposed explanation also suggests that MSBA should be a poor stabilizer for particles surface. This was confirmed after comparing stability results for prepared NbNP of solutions using MSBA and I-907. After three month of bench storage, TEM results identified no changes to the particles prepared using I-907, but the particles with just MSBA underwent noticeable aggregations. Such aggregation shows that MSBA is unable to provide long term protection for the surfaces of NbNP.

2.6 Experimental Details

The experimental procedure was adopted from the published work that is dedicated to this thesis.[4]

General

Unless otherwise stated, all chemicals used for sample preparation were purchased from Sigma-Aldrich in the highest purity available and used as received. Irgacure 907 was a generous gift obtained from Ciba Specialty Chemicals (now BASF Global). HPLC grade CH_3CN was purchased from Sigma Aldrich and purified using a LC Technologist Solvent Purification System fitted with an alumina column. All glassware was thoroughly cleaned, rinsed with nanopure water and dried at 130°C prior to use. Hot glassware was immediately sealed and purged with Industrial T (99.9%) argon gas after removal from the oven.

Preparation of acetylacetone stabilized Nb (V) ($Nb(acac)_5$) stock solution

A 208 mM stock solution of $Nb(acac)_5$ was prepared by simple ligand exchange with Nb (V) ethoxide in an amber vial. In a glove box under N_2 atmosphere, 2.0 mmol (0.5 mL) of niobium (V) ethoxide was added to 1.6 mL of CH_3CN followed by 10.7 mmol (1.1 mL) of acetylacetone and diluted to a final volume of 9.6 mL. The vial was sealed and allowed to stand for 20-30 minutes to allow for complete ligand exchange. The stock solution was stored under argon at -10°C between uses.

Preparation of 500 mM Irgacure 907 (I-907) stock solution

A 500 mM stock solution was prepared by dissolving 1.40 g of I-907 in 10 mL of CH_3CN. The solution was stored in a 15 mL amber vial under argon at room temperature to prevent photodegradation. The presence of the acetylacetonate ligand was confirmed by Raman spectroscopy, where the presence of Raman shifts at 260 cm-1 (broad), 430 cm-1 and 880 cm-1 were indicative of ethanol release upon successful acac ligand exchange. (**Figure 2.1**)

Preparation of 4-(methylthio)benzaldehyde (MSBA) stock solution

A 0.5 M stock solution was prepared by dissolving 0.66 mL of MSBA into 10 mL CH_3CN. The mixture was stored under Ar gas at room temperature inside the sealed 15 mL amber vial.

Synthesis and stock solution preparation of isopropylmorpholine

N-isopropylmorpholine was synthesized and purified according to a previously reported method (Yamashiro, D., Li, C.H. *Int. J. Peptide Protein Res.* **1988**, *31*, 322-334). A 0.5 M stock solution of isopropylmorpholine in CH_3CN was then made for use in subsequent experiments.

NbNP Sample Preparation

10.4 μM of $Nb(acac)_5$ (1.0 μL of 280 mM stock solution; 0.25μmol) and varying concentrations of I-907 (using 500 mM stock solution; 60, 80, 100, 190, 260, 420, 520, 620, 730 μM) were added to 20 mL of CH_3CN in a 50 mL round bottom flask. The reaction mixture was shaken thoroughly, separated into the six 7 mm × 7 mm quartz cuvettes and irradiated for 300 min at 24 °C inside a Luzchem photoreactor equipped with 14 UVB blubs (λ=281-315 nm; 62 W/m2). Samples were rotated to allow for homogeneous irradiation of the solutions.

Instrumentation

UV-visible spectra were carried out on a Cary 50 spectrophotometer. Samples were measured in the 7 mm × 7mm quartz cuvettes in which they were prepared (no sample dilution) and under argon or atmospheric conditions, as indicated.

The size of NbONP were determined using a JSM-7500F field emission scanning electron microscope (SEM) from JEOL Ltd. NbONP size was determined from an average of 150-200 particle measurements.

Raman spectra were collected using a single mode 785 nm laser (Innovative Photonic Solutions) with a maximum power output of 100 mW. The laser beam was passed through a band pass filter centred at 785 nm to filter out wavelength components in this wavelength region

from the laser diode. A dichroic filter (R785RDC, Chroma Technologies Corp.) was use to reflect the light at an angle of 45° onto the sample and was further focused using a 40x microscopic objective lens.

The Raman light was collected by a fiber bundle (Fiberoptic System Inc., 26 multimode fiber) coupled to a Kaiser f/18i Spectrograph with a CCD camera. Andor SOLIS software was used for spectral data acquisition. Samples used for Raman spectroscopy were prepared as described using the aforementioned substrate concentrations in a 7 mm × 7 mm quartz laser cuvette under argon atmosphere.

2.7 Appendix

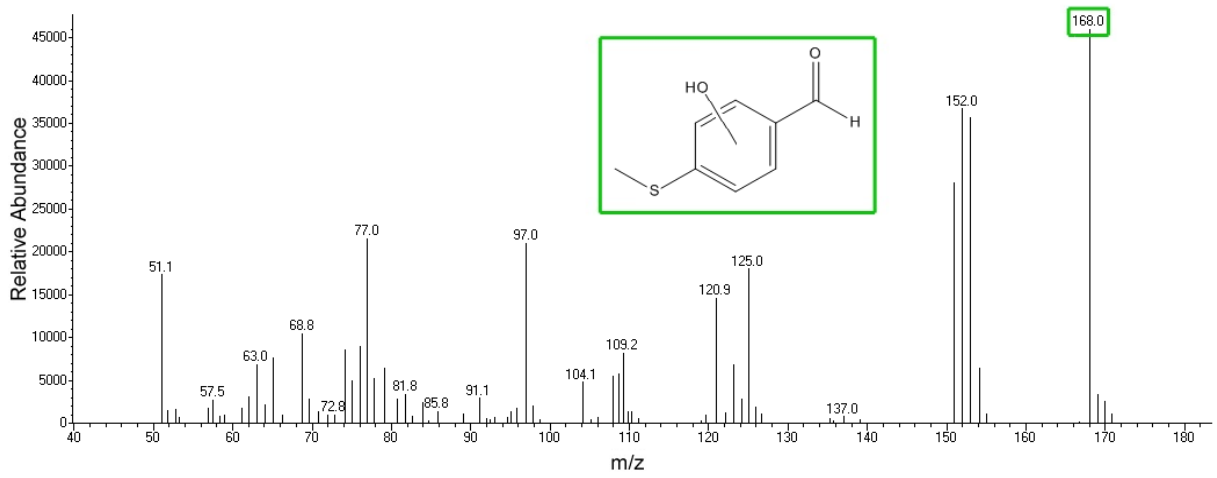

App. Figure 1.1 Mass spectrum of 4-(methylthio)benzoic acid (MSCOOH).

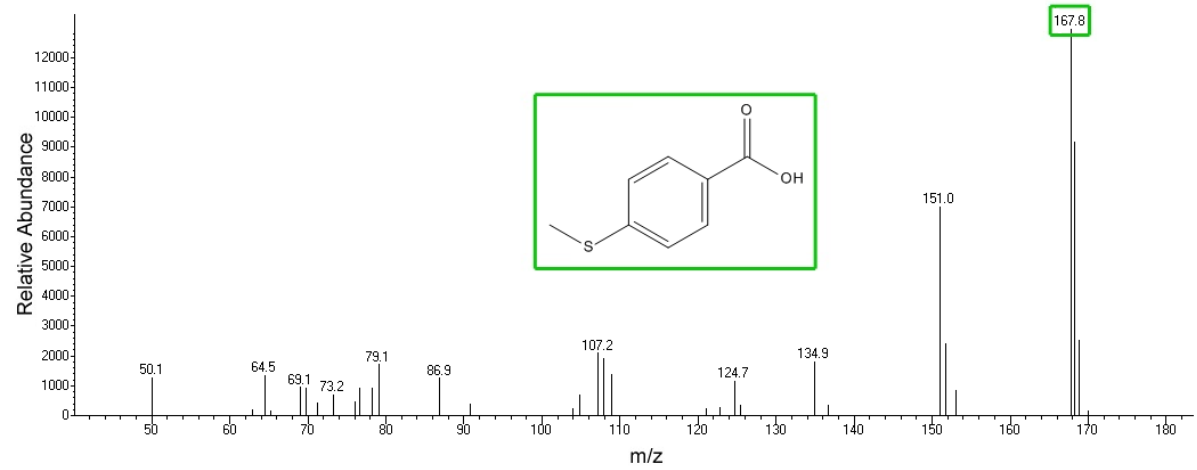

App. Figure 2 Mass spectrum of 4-(methylthio)benzaldehyde (MSBA).

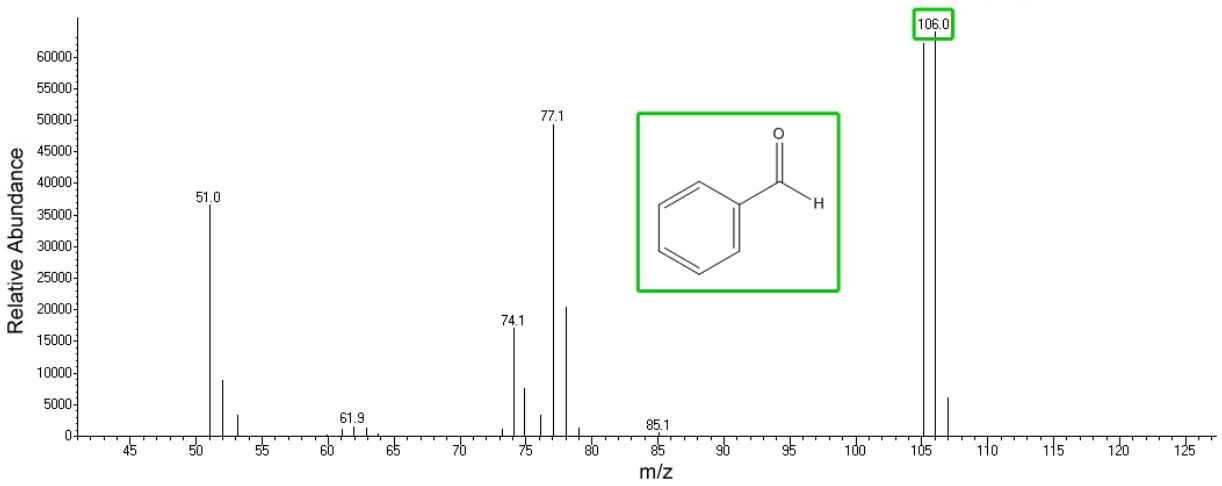

App. Figure 3 Mass Spectrum of benzaldehyde (BA).

2.8 References

1. McGilvray, K. L.; Fasciani, C.; Bueno-Alejo, C. J.; Schwartz-Narbonne, R.; Scaiano, J. C., *Langmuir* **2012,** *28* (46), 16148-16155.
2. Pacioni, N. L.; Filippenko, V.; Presseau, N.; Scaiano, J. C., *Dalton transactions* **2013,** *42* (16), 5832-8.
3. Danial D.M.; Wayner, J. J. D.; David Griller., *Chemical Physics Letters* **1986,** *131* (3).
4. Malyshev, D.; Bosca, F.; Crites, C. O.; Hallett-Tapley, G. L.; Netto-Ferreira, J. C.; Alarcon, E. I.; Scaiano, J. C., *Dalton transactions* **2013,** *42* (39), 14049-52.
5. Giuffrida, S.; Ventimiglia, G.; Sortino, S., *Chem Commun* **2009,** (27), 4055-4057.
6. Sedlar, M.; Sayer, M., *J Sol-Gel Sci Techn* **1995,** *5* (1), 27-40.
7. Scaiano, J. C.; Stamplecoskie, K. G.; Hallett-Tapley, G. L., *Chem Commun* **2012,** *48* (40), 4798- 4808.
8. McGilvray, K. L.; Decan, M. R.; Wang, D.; Scaiano, J. C., *J.A.C.S.* **2006,** *128* (50), 15980-1.
9. Stamplecoskie, K. G.; Scaiano, J. C., *Photochem Photobiol* **2012,** *88* (4), 762-768.
10. Scaiano, J. C.; Netto-Ferreira, J. C.; Alarcon, E.; Billone, P.; Alejo, C. J. B.; Crites, C. O. L.; Decan, M.; Fasciani, C.; Gonzalez-Bejar, M.; Hallett-Tapley, G.; Grenier, M.; McGilvray, K. L.; Pacioni, N. L.; Pardoe, A.; Rene-Boisneuf, L.; Schwartz-Narbonne, R.; Silvero, M. J.; Stamplecoskie, K. G.; Wee, T. L., *Pure Appl Chem* **2011,** *83* (4), 913-930.
11. Scaiano, J. C., Stamplecoskie, K. G., McGilvray, K. L. and Pacioni, N. L., In *Encyclopedia of Radicals in Chemistry, Biology and Materials.* 2012.
12. Brown, K. R.; Walter, D. G.; Natan, M. J., *Chem Mater* **2000,** *12* (2), 306-313.
13. Esen, D. S.; Arsu, N.; Da Silva, J. P.; Jockusch, S.; Turro, N. J., *J Polym Sci Pol Chem* **2013,** *51* (8), 1865-1871.
14. Scaiano, J. C.; Aliaga, C.; Maguire, S.; Wang, D., *J.Phys.Chem* **2006,** *110* (26), 12856-9.
15. Eustis, S.; Krylova, G.; Eremenko, A.; Smirnova, N.; Schill, A. W.; El-Sayed, M., *P.P.S.*, **2005,** *4* (1), 154-9.
16. Marin, M. L.; McGilvray, K. L.; Scaiano, J. C., *Journal of the American Chemical Society* **2008,** *130* (49), 16572-84.
17. Filipiak, P.; Hug, G. L.; Bobrowski, K.; Marciniak, B., *J.Photoch. Photobio* **2005,** *172* (3), 322-330.
18. Hostetler, M. J.; Wingate, J. E.; Zhong, C.-J.; Harris, J. E.; Vachet, R. W.; Clark, M. R.; Londono, J. D.; Green, S. J.; Stokes, J. J.; Wignall, G. D.; Glish, G. L.; Porter, M. D.; Evans, N. D.; Murray, R. W., *Langmuir* **1998,** *14* (1), 17-30.
19. Kell, A. J.; Alizadeh, A.; Yang, L.; Workentin, M. S., *Langmuir* **2005,** *21* (21), 9741-9746.

3 • Characterization of Niobium Oxide Nanoparticles: *Catalytic Investigation*

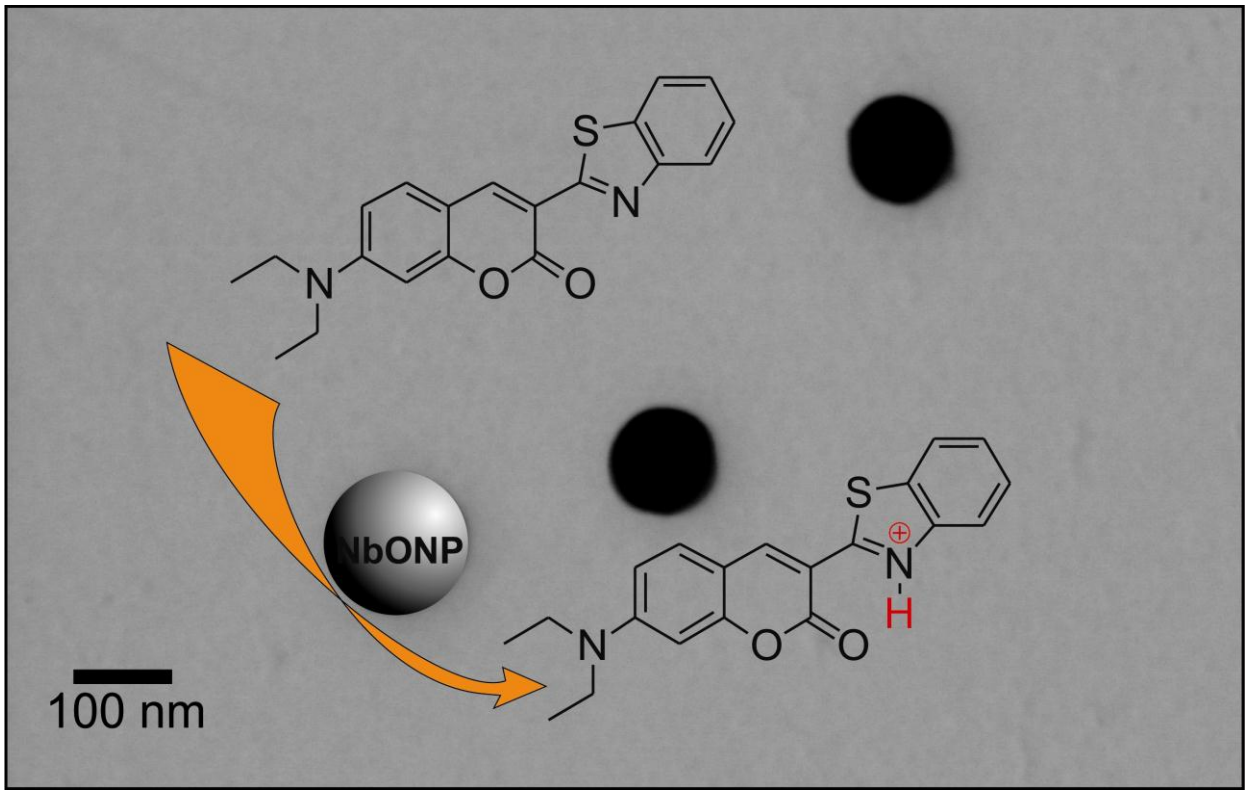

Cover Image designed and created by Dimitriy Malyshev.

(Actual TEM image of NbNP with an illustrative design of C6 protonation.)

3.1 Characterization of NbONP

In chapter 2, we developed a method for the size controlled synthesis of NbONP. Here we will take a full advantage of this method for the synthesis of large NbONP (with a mean size 110 nm) to perform their structural characterizations. In addition to their characterizations, varying sizes of NbONP (previously synthesized, see Chapter 2) are used here for the experiment in determining the relationship between the size dependence and the Brønsted acidity of the nanoparticles.

Note: the characterization techniques that are being used, such as P-XRD, XPS and EDS provide a higher reliability in obtaining data for the larger size nanoparticles than for small ones. It is also easier to isolate and purify larger particles (via centrifugation) than the small ones.

3.1.1 Structural Analysis of NbONP

3.1.2 Amorphousness of NbONP (TEM and P-XRD)

Depending on the conditions during synthesis, nanoparticles may form into either crystalline or amorphous state. It is known that crystalline nanoparticles possess a well-defined arrangement of atoms in the form of the crystal lattice on particles' surface. In contrast, amorphous nanoparticles possess disordered structures that are often porous due to multiple structural defects on their surface.[1]

The crystalline and amorphous states may provide their own unique advantage for catalytic applications. For example, many crystalline nanoparticles are involved in stereospecific catalytic reactions that amorphous nanoparticles often lack.[2] However, while lacking stereo-specificity, amorphous nanoparticles possess a higher catalytic efficiency than the crystalline ones.[3,4] This effect is primarily due to more catalytic sites that are available on the porous surface of amorphous nanoparticles.[4] Therefore, it is important to characterize the structure of NbONP being formed, for it will provide an insight into the future catalytic investigations.

TEM was used to help determine the structural characteristics of NbONP. It was found to be a reliable method to study the particle shapes and to evaluate their sizes. We decided to use TEM, but in combination with method of selected area electron diffraction (SAED). SAED provided insight about the state of particles (crystalline or amorphous), using only a small amount of a sample.

The synthesis of large (a mean size of 110 nm) NbNP was conducted using 420 μM $Nb(acac)_5$ and 10 mM I-907 (experimental details, see Chapter 4). These NbNP were exposed to air and centrifuged (10000 rpm) and re-suspended three times in acetonitrile to remove any excess organic materials prior to their deposition on the copper grid. **Figure 3.1** shows the projected TEM image of these particles.

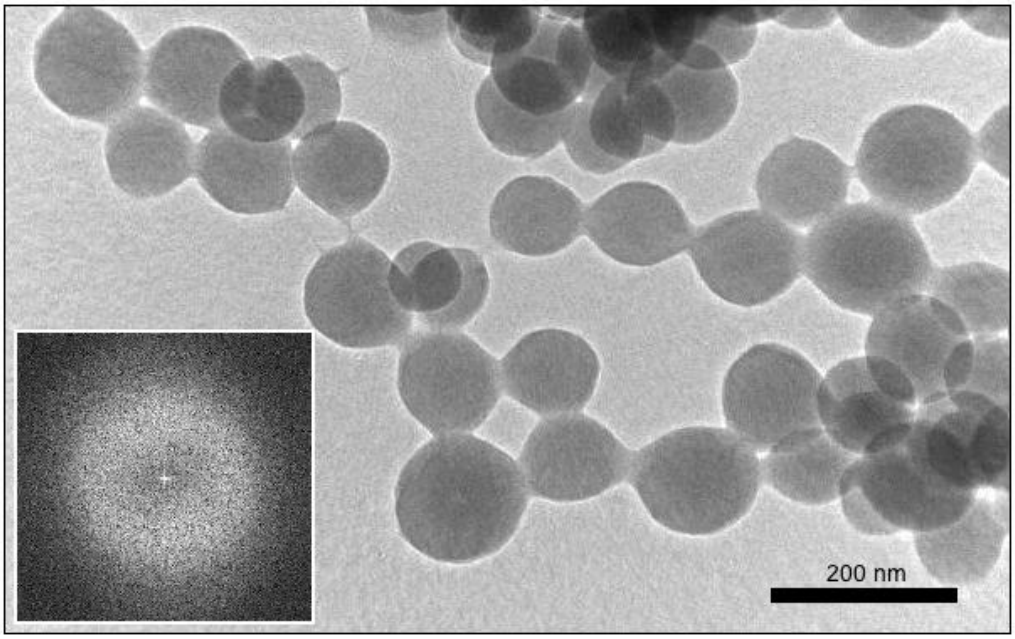

Figure 3.1 TEM of NbONP prepared from a solution of 420 µM I-907 and 10 mM $Nb(acac)_5$. Inset depicts diffraction pattern of these particles using SAED.[5]

Figure 3.1 illustrates SAED of NbONP. In the inset of **Figure 3.1**, the broad diffusive ring suggests an amorphous state of the nanoparticles. Since the SAED pattern is only being related to a small number of particles involved, it is a limitation to this method. An indirect approach can be used to confirm the amorphous state of NbONP, such as monitoring of their thermal and magnetic behaviours.[6] However, attempts to use these two additional methods provided no conclusive results. Therefore, an X-ray Diffraction (XRD) analysis was performed to confirm an amorphous state of NbONP. **Figure 3.2** illustrates results of Powder-XRD pattern for the same sample that was used in SAED.

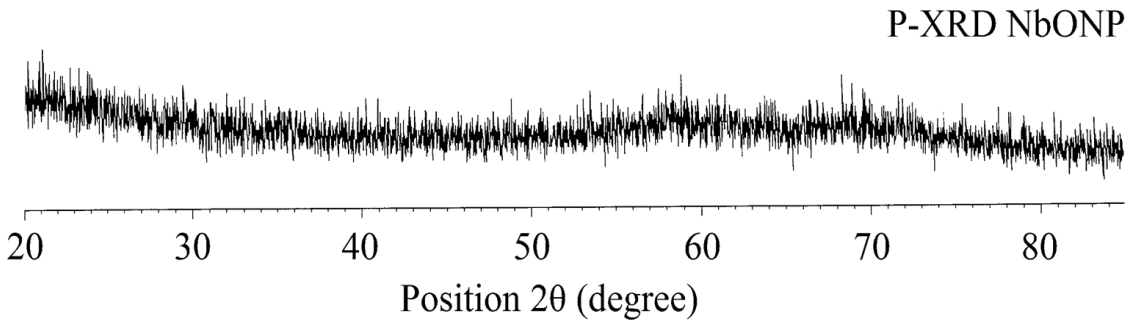

Figure 3.2 P-XRD pattern of NbONP as powder, prepared from a solution of 420 µM I-907 and 10 mM $Nb(acac)_5$.

The absence of Bragg peaks in **Figure 3.2** is a confirmation of the amorphous state of the NbONP sample. In the crystalline samples, diffraction peaks should appear.[6] In conclusion, the experimental results of both SAED (with TEM) and P-XRD investigations demonstrated that the NbONP synthesized via the photochemical approach are amorphous.

3.1.3 Core-Shell of NbONP (HRTEM)

Upon exposure to air, NbNP undergo a rapid oxidation that converts niobium into higher-oxidation state, Nb(V). However, this assumption is valid only if NbNP are formed initially with the lowest oxidation state (metallic) during their synthesis. If that is the case, then we can predict that NbONP should have structure of a core-shell particle. Where the shell is in its highest oxidation state of Nb_2O_5 and the core is in metallic Nb^0, as illustrated in graphic representation (left) of **Figure 3.3**.

To investigate the structure of NbONP we used the high resolution TEM imaging (HRTEM) technique. HRTEM is a reliable method to study the morphology of projected interface, as well evaluate its roughness and predict its relative density. **Figure 3.3** (right image) shows the projected HRTEM image of individual particle.

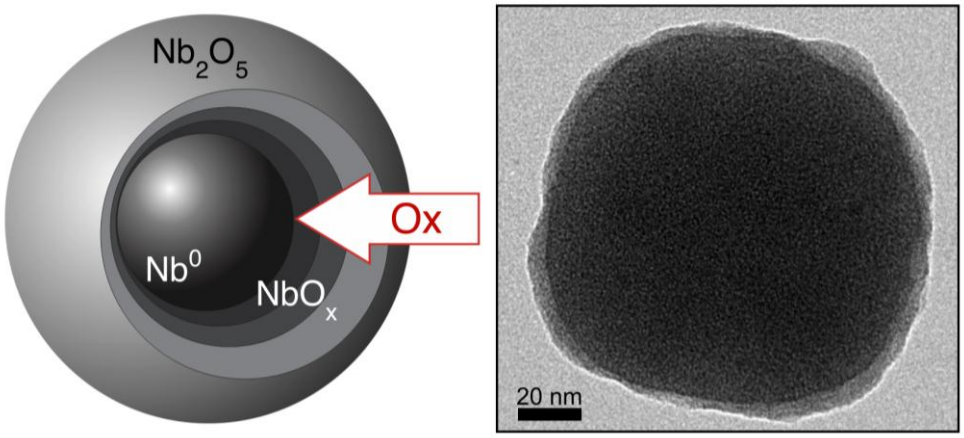

Figure 3.3 Graphic representation of the surface oxidation of NbNP (left). Representative HRTEM image of NbONP (420 µM $Nb(acac)_5$ and 10 mM I-907) depicting a rough 5-10 nm Nb oxide shell (right).[5]

The examination of the HRTEM image of NbNP (**Figure 3.3**) shows a rough surface shell covering the surface of this particle. Such projected contrast between the outer shell and the inner core indicates that the densities of the two parts differ. This difference in the density implies the difference in composition and the different oxidation states of the metal (left, **Figure 3.3**).[7] Therefore, this experiment shows the formation of metallic (Nb^0) NbNP (under dry condition) and their transformation to the two-layered NbONP when exposed to dioxygen. To further study surface of this sample, an elemental analysis using Energy Dispersive X-ray spectroscopy (EDS) was used.

3.1.4 EDS Analysis of NbONP

Both TEM and HRTEM were collected using JEOL JEM-2100F field emission transmission electron microscope (operating at 200kV).[5] Furthermore, Oxford Instrument X-Ray EDS was attached to JEM-2100F microscope. **Figure 3.4** illustrates chemical analysis collected from the sample of NbONP (prepared from solutions of 420 μM $Nb(acac)_5$ and 10 mM I-907).

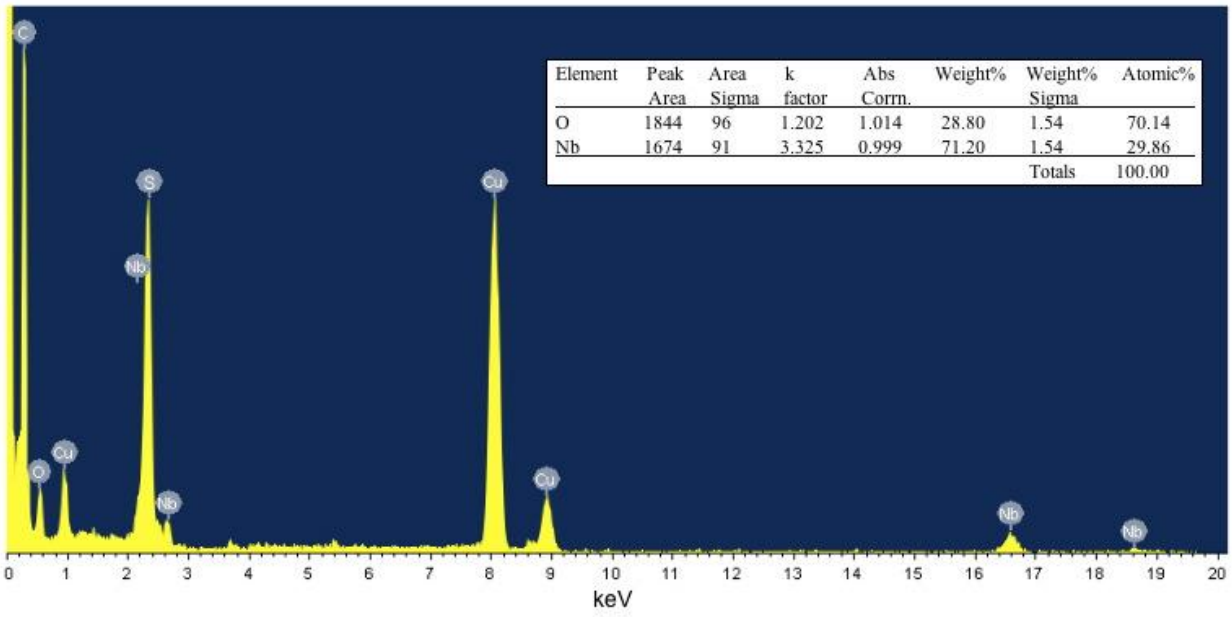

Element	Peak Area	Area Sigma	k factor	Abs Corrn.	Weight%	Weight% Sigma	Atomic%
O	1844	96	1.202	1.014	28.80	1.54	70.14
Nb	1674	91	3.325	0.999	71.20	1.54	29.86
						Totals	100.00

Figure 3.4 EDS analysis of NbONP (420 μM $Nb(acac)_5$ and 10 mM I-907). Note the results on atomic % for O and Nb, (5/2), confirming Nb_2O_5 formation on the particles` surface.[5]

The results of EDS analysis (**Figure 3.4**) demonstrated the composition of 30% Nb and 70% O, therefore suggesting that the outer shell of NbONP are Nb_2O_5 in its composition. These EDS results are consistent with the literature values.[8]

While EDS can provide a high accuracy and sensitivity, it also has a limitation to the short probing depth (<10 nm) for the chemical analysis.[9] As a consequence, we cannot probe the composition of the NbONP core. Thus, we used the X-ray photoelectron spectroscopy (XPS) and ionic sputtering to probe the core.

3.1.5 XPS Analysis of NbONP

NbONP were examined using XPS sputtering technique. In this technique, a sample of NbONP is first analysed with XPS and then is followed by an ionic sputtering. As illustrated in **Figure 3.5**, the ionic sputtering bombards the surface of NbONP to peel off the top layers to reveal their chemical composition and the Nb core.

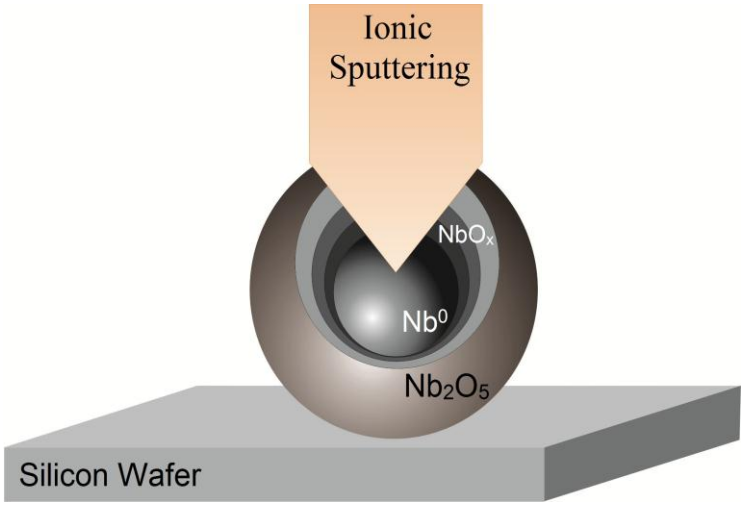

Figure 3.5 Graphical representation of XPS sputtering of NbONP powder prepared on the silicon wafer (420 µM $Nb(acac)_5$ and 10 mM I-907).[5]

After the sputtering, the XPS analysis was done again (the XPS chamber is kept under vacuum) to probe the chemical composition of the NbONP core. The XPS spectra of NbONP before and after sputtering are compared in **Figure 3.6**.

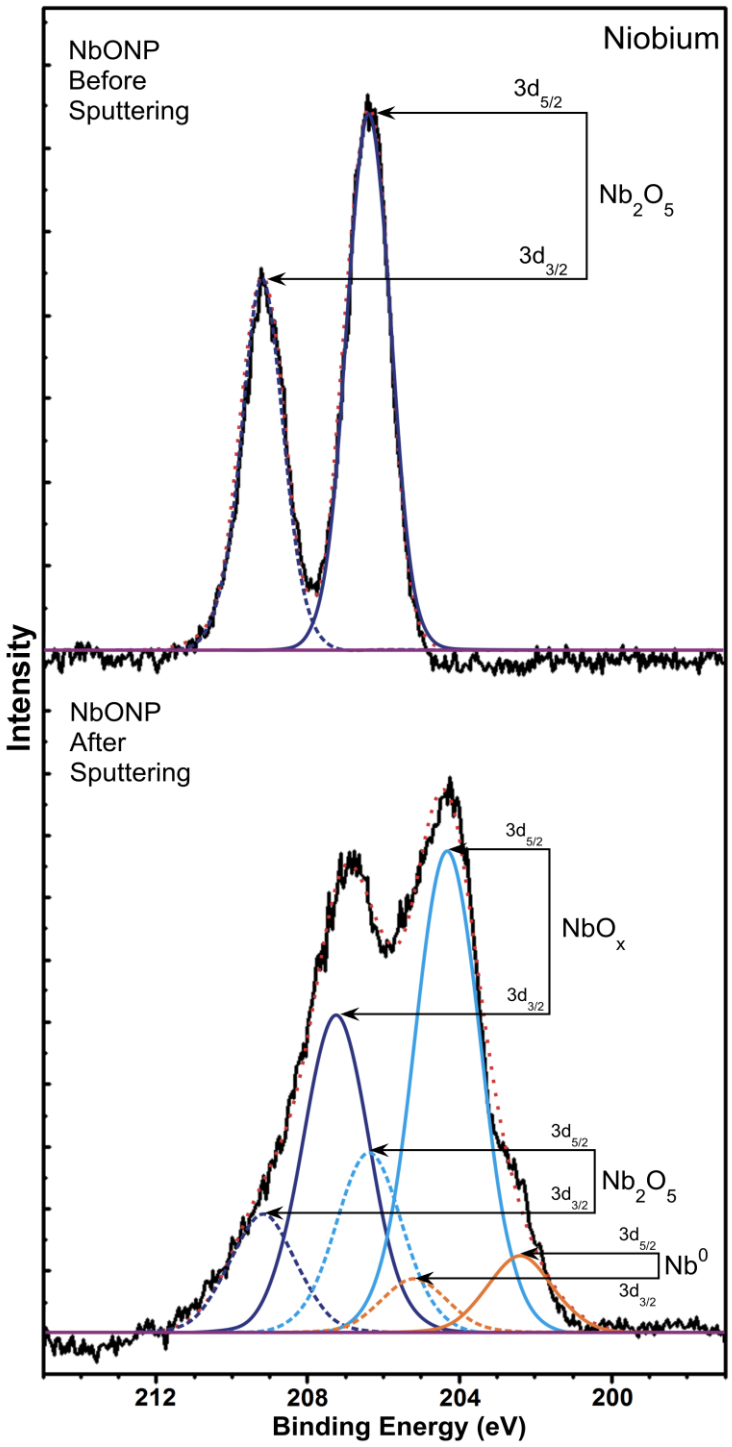

Figure 3.6 XPS spectra of NbONP (420 µM $Nb(acac)_5$ and 10 mM I-907) before and after ionic sputtering.[5] Note the formation of peaks of Nb^0 after the sputtering took place.

The XPS spectrum before sputtering illustrates the presence of an initial surface shell of Nb_2O_5. This is suggested by the presence of two binding energies of 209.2 and 206.4 eV, and a doublet split of 2.8 eV with an intensity ratio of 1.5 for $3d_{5/2}/3d_{3/2}$.[10,11] Following this measurement, an XPS sputtering was performed for 30 minutes.

As seen in **Figure 3.6**, after the sputtering, the XPS spectrum shows a shift in electron binding energies and a change in its overall spectral shape. The Nb_2O_5 doublet that is seen in the spectrum before sputtering shifts approximately 4 eV, indicating the presence of a mixture of NbO_x species with a lower oxidation state of the metal.[5,10,11] Moreover, the band analysis of the Nb/O ratio before and after XPS sputtering shows an increase in the contribution of Nb to the nanoparticle composition from 0.4 to 3.9 (See Appendix 3.3). Such an increase is associated with the presence NbO_x, including Nb^0, beneath the outer Nb_2O_5 shell.[5] A small shoulder at 202.4 eV is attributed to the Nb^0 metal core.[11]

At the time of these XPS results, it was a possibility that ionic sputtering might cause a reduction of the NbONP surface and thus misguide that there is a metallic core. To prove that ionic sputtering does not cause problems, a commercially available Nb_2O_5 catalyst (obtained from CBMM, Brazil) was used as a control for the same XPS sputtering experiment, see results in **Figure 3.7**.

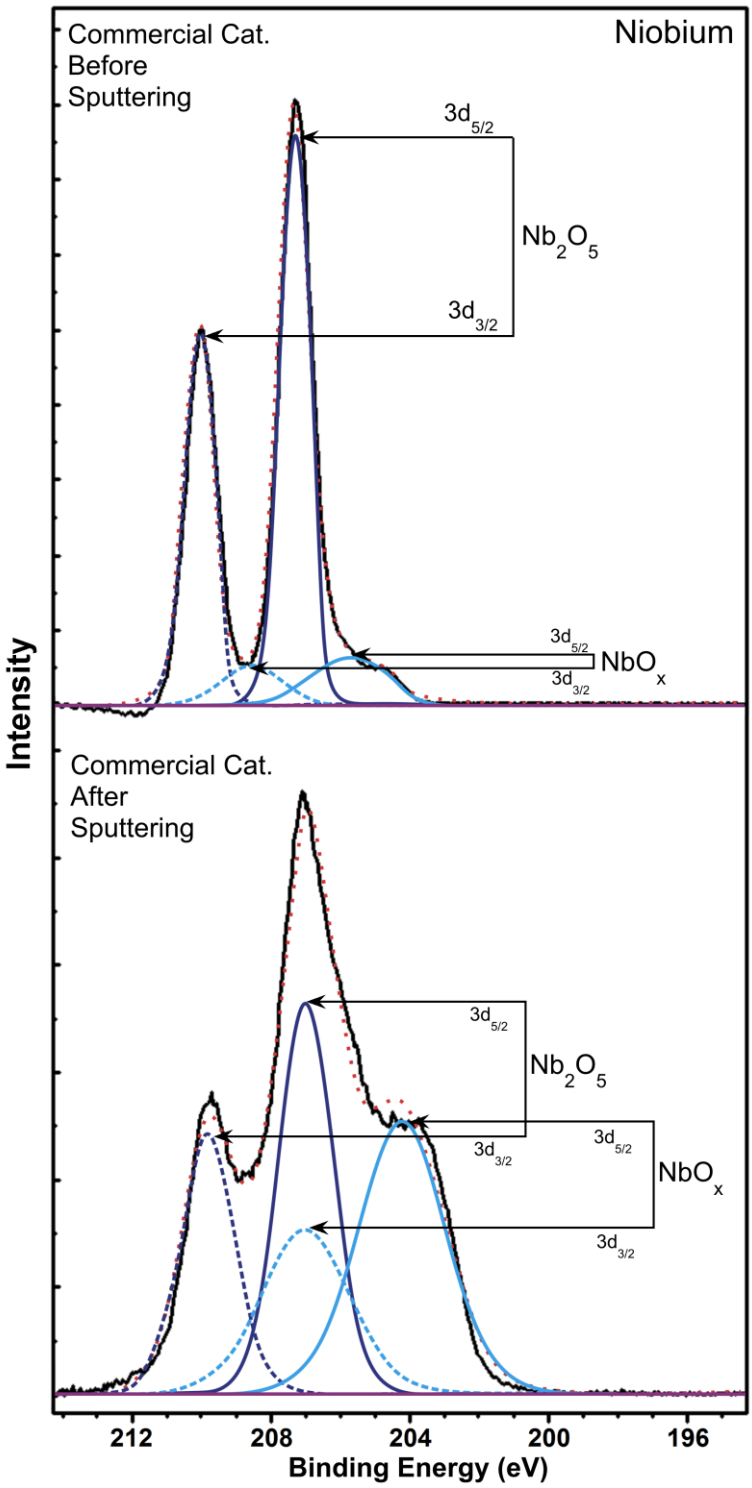

Figure 3.7 XPS spectra of commercial Nb_2O_5 catalyst (obtained from CBMM, Brazil) before and after ionic sputtering.[5] Note the lack of Nb^0 after sputtering.

As seen in **Figure 3.7**, after the sputtering of commercial Nb_2O_5 catalyst, there was no indication of the Nb^0 metal as was found in results of NbONP. However, the sputtering of this material demonstrated that other NbO_x species are present under the Nb_2O_5 surface. When the XPS band intensities between NbO_x and Nb_2O_5 are compared for the commercial catalyst to NbONP, it becomes apparent at how much less Nb_2O_5 are being present in the composition of NbONP (that is only on its surface). The results of this experiment removed any doubts that sputtering of Nb_2O_5 might cause reduction (to produce Nb^0), and provided a positive feedback to the performed characterization of NbONP.

For the synthesis of NbONP we used $Nb(acac)_5$ as a niobium precursor. Since the acac ligand has two oxygen atoms within its structure, it is possible (despite the evidence for the metallic core), that the formation of the Nb_2O_5 outer shell occurs at the end of the synthesis is due to residual amounts of $Nb(acac)_5$. To confirm that Nb^{5+} is not due to the presence of residual $Nb(acac)_5$, we analysed 1s C region of the XPS data both before and after sputtering (**Figure 3.8** and Appendix 3.4).

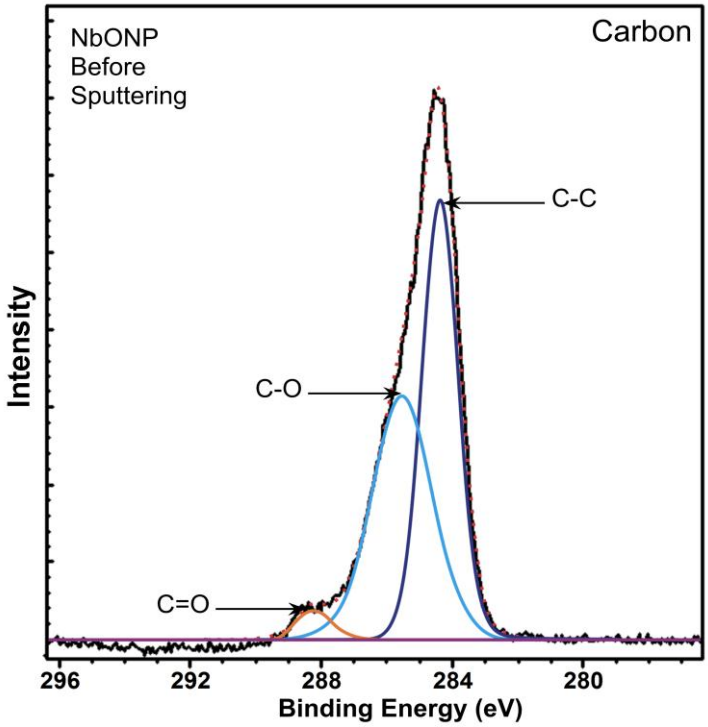

Figure 3.8 XPS analysis of 1s C region of NbONP (420 µM $Nb(acac)_5$ and 10 mM I-907) before sputtering.[5]

Analysis of the 1s C region for both before (**Figure 3.8**) and after sputtering (Appendix 3.4) illustrated an insignificant presence of C–O (285.5 eV) and C=O species (288.3 eV). These XPS results confirm that Nb^{5+} is in the form of Nb_2O_5 and are not formed due to the presence of residual $Nb(acac)_5$ starting material, but to its exposure to the atmospheric air.

3.2 Catalytic properties of NbONP

3.2.1 Brønsted acidity of NbONP (Coumarin-6 dye)

The data obtained from the XPS experiments illustrated that NbONP has a shell-core structure, where the core is primarily composed of Nb^0 and the shell of Nb_2O_5. Under wet conditions, such Nb_2O_5 surface reacts with water to become an active niobic acid [$HNbO_3$]. The identity of niobic acid is characterized by its structural composition. For example, a crystallized (calcined at 773K) niobic acid was found to show a Lewis acidity, whereas an amorphous structure (calcined at ≤373K) a Brønsted acidity.[12] Furthermore, it was reported that amorphous niobic acids possess a very strong acidic character of $H_o < -5.6$.[12]

TEM imaging projected a roughness to the shell surrounding the surface of NbONP, since it has an amorphous structure we can predict that it will possess a Brønsted acidity and not a Lewis acidity. To investigate this proposal we used coumarin-6 (C_6), as a pH sensitive dye as probe for Brønsted acidity.[13,14] C_6 gets protonated under Brønsted acid conditions that can be observed using UV-visible absorption and fluorescence spectroscopy.[15] Using C_6 as a probe, a variety of differently sized NbONP were tested for Brønsted acid activity, as seen in **Table 3.1**.

Table 3.1 Mean size of NbONP and their acitivity on Protonation of Coumarin-6 dye.

Mean size of [91 fM] NbONP (In acetonitrile)	**Protonation of [0.9 µM] Coumarin- 6** (Fluorescence spectrometry)
10.4 nm (60 µM I-907)	No activity
27 nm (100 µM I-907)	No activity
43 nm (190 µM I-907)	Low activity
67 nm (260 µM I-907)	**High intensity of protonation**
110 nm (420 µM I-907)	Low intensity of protonation

Results of fluorescence experiments, illustrated that even with the subpicomolar concentration, NbONP were able to protonate up to 0.9 µM of C6. Furthermore, the highest intensity of formation of protonated coumarin-6 was observed for the particles with the mean size of 67 nm, as seen in **Figure 3.9**.

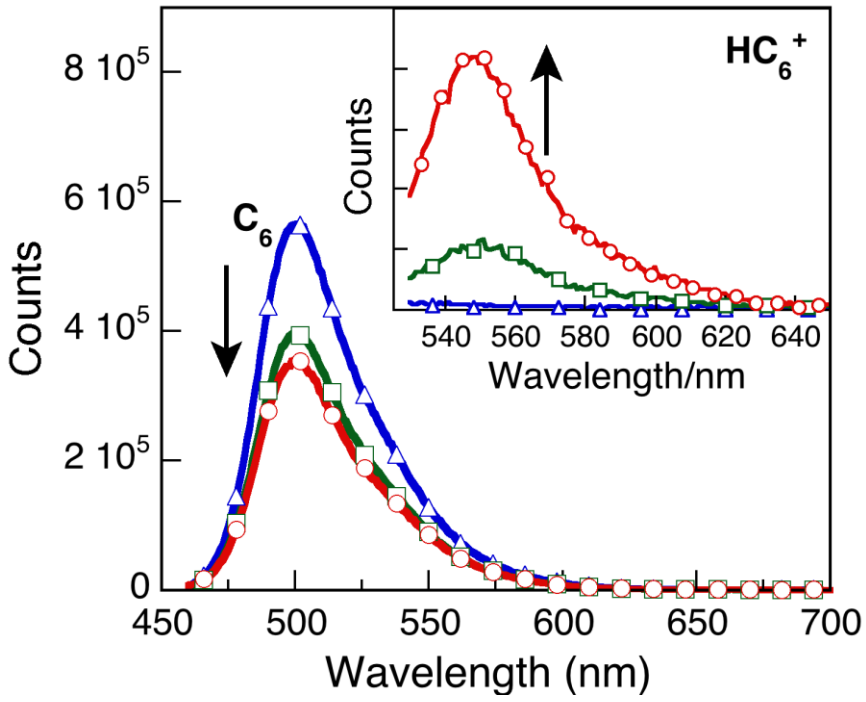

Figure 3.9 Fluorescence emission spectrum of a 0.9 µM C_6, control (Δ), 0.9 µM C6 in the presence of 91 fM (□) and 0.4 pM (○) NbONP. NbONP were prepared using 260 µM I-907 and 10 µM $Nb(acac)_5$. Addition of C_6 into solutions NbONP resulted in an immediate decrease in the intensity of C6 emission (λemit = 500 nm, λex = 450 nm). Inset presents an increase in emission at λemit = 555 nm (λex = 520 nm) of the C6 protonated form (HC6+).[5]

Figure 3.9 illustrates results of fluorescence emission for protonation of C6 (to a final 0.9 µM concentration) with NbONP. The fluorometry analysis was performed using two concentrations of NbONP (mean size of 67 nm), 91 fM and 0.4 pM,. As the concentration of NbONP increases, the concentration of protonated C6 also increases; these results were further confirmed using absorbance spectroscopy, **Figure 3.10**.

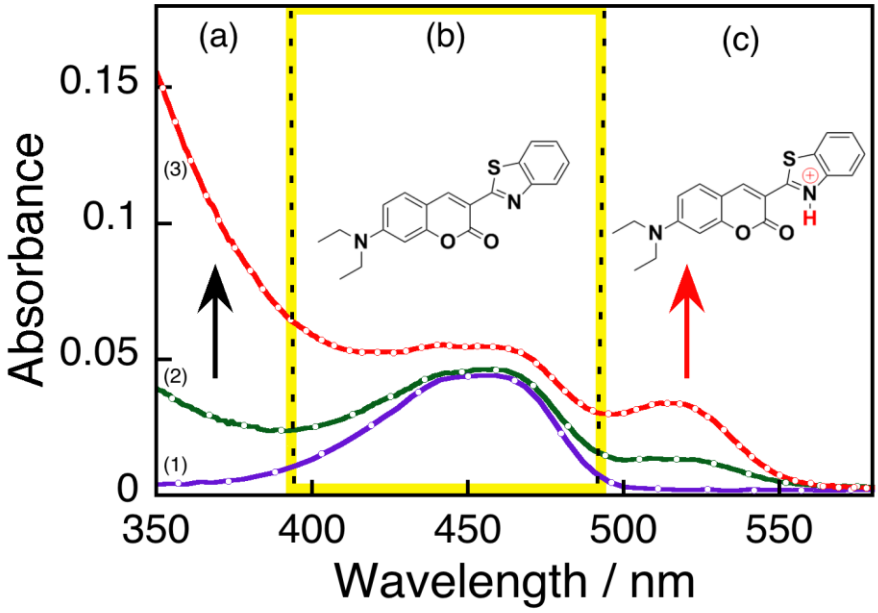

Figure 3.10 UV-Vis absorption spectra obtained for the samples containing 0.9 µM of C6 with (1) 0 nM, (2) 91 fM and (3) 0.4 pM of 85 ± 15 nm NbONP. Three areas are highlighted to represent the major, light-absorbing species in the reaction: (a) NbONP (light scattering), (b) non-protonated coumarin-6, and (c) protonated C_6.

As seen from the absorption spectra in **Figure 3.10**, with the increasing concentration of NbONP, the absorption band of protonated C6 increases (**(c)** of **Figure 3.10)**. Although the absorption spectra confirm the formation of protonated C6, it is difficult to see if there is decrease in the absorbance of non-protonated C6 (**(b) Figure 3.10),** as it was seen in the fluorescence emission in **Figure 3.9**. This might be partially due to the presence of NbONP that causing a light scatter, which generates a noise for the accurate measurement, as seen with the shift in baseline on the right **(a)** in **Figure 3.10.**

3.3 Discussion and Summary

Characterization of NbONP has illustrated the core-shell structure of the nanoparticles. Furthermore, the XPS results indicated that the core is metallic Nb^0 and the shell is the niobium oxide, Nb_2O_5. Since, NbONP are amorphous and their shell is composed of Nb_2O_5, we designed an experiment to test the Brønsted acidity of the nanoparticles with Coumarin-6.

Experiments using C_6 illustrated a strong Brønsted acidity for a large sized NbONP (**Table 3.1**). Surprisingly, there was little to no activity when using smaller size particles. This observation could be attributed to the competitive quenching of their active sites with the water. (The prepared stock solution of C6 does not dissolve well in Acetonitrile; an addition of small amount ~10% of water promotes its solubility.)

For example, some reports have indicated a high reactivity of niobium oxide in the dehydration of alcohols, such as 2-butanol, 2-propanol, and cyclohexanol.[16,17] However, the

success for dehydration was found to be majorly depended on the amount of water present in the reaction solution.[17] Work by Fraissard *et al.* demonstrated that the theoretical number of protons per gram of hydrated niobium ($H_2Nb_6O_{16}$) is 1.6 x 10^{21}. [18,19] This estimates that there are only two hydroxyl groups per unit cell of niobic acid.[12] Furthermore, as the number of coordinated water molecules increases the number of available Brønsted acid sites for alcohols to bind decreases. Water gets adsorbed on the surface of niobium hindering access to the active sites for the other molecules, and instead produces hydronium ions (H_3O^+). It was reported that there are a linear correlation between the concentration of H_3O^+ produced to the number of adsorbed water.[12]

Dehydration of alcohols using NbONP could be an excellent method for testing Brønsted acid sites. However, it is difficult to perform such experiment unless NbONP are produced in higher amounts, because in its current subpicomolar concentration ($\leq$ 91 fM) the active sites of NbONP could be easily suppressed with even smallest contamination of water. This may be one of the reasons why there was a low protonation of C6 with small size particles. Given these points, production of NbONP in greater amounts is very important for the future studies (Chapter 4).

3.3 Experimental Details

The experimental procedure was adopted from the published work.[5]

Instrumentation

The size of NbONP were determined using a JSM-7500F field emission scanning electron microscope (SEM) from JEOL Ltd. NbONP size was determined from an average of 150-200 particle measurements.

Both TEM and HRTEM were collected JEOL JEM-2100F field emission transmission electron microscope equipped with an ultra high-resolution pole-piece operating at 200kV. Elemental analysis of the NbONP was accessed using an Oxford Instruments X-ray energy dispersive spectrometer (EDS) attached to the JEM-2100F microscope. Solutions for SEM were prepared by dropping 10 mL of the reaction mixture onto a copper grid. For TEM analysis, samples were centrifuged (10000 rpm) and re-suspended in CH_3CN to ensure removal of any excess organic materials prior to deposition on the copper grid.

X-ray photoelectron spectroscopy (XPS) was recorded using Kratos analytical model Axis Ultra DLD, using monochromatic aluminum Ka X-rays at a power of 140 watts. XPS samples were prepared by dropping 20 mL of sample onto a 1 cm × 1 cm silicon wafer and the solvent was evaporated prior to analysis.

XPS spectra on fresh NbONP powders were recorded on a Kratos analytical model Axis Ultra DLD using monochromatic aluminium Ka X-rays at a power of 140 watts. XPS sputtering was achieved using Ar ion impact at 4 keV for 30 minutes using θ =45°. Measured sample currents were 1 μA over a 4 mm × 4 mm area using a flood gun calibrated for optimal peak shape and C-C carbon as the reference photoelectron for charge accumulation correction. XPS data was analyzed using CasaXPS software, Version 2.3.15 and all fittings obtained using a Gaussian/30% Laurentian and a Shirley baseline.

3.4 Appendix (XPS results)

Table 2.2 Combined data of XPS analysis.

a) NbONP; Nb analysis (before sputtering)

Peak Identity	Peak Type	BE (eV)	FWHM	R.S.F	Fit	Area	% Area
Nb_2O_5	$3d_{5/2}$	206.4	1.32	8.21	GL(30)	1865	59.5
	$3d_{3/2}$	209.2	1.32	8.21	GL(30)	1270	40.5

b) NbONP; Nb analysis (after sputtering)

Peak Identity	Peak Type	BE (eV)	FWHM	R.S.F	Fit	Area	% Area
Nb_2O_5	$3d_{5/2}$	206.4	2.23	8.21	GL(30)	1284	14.7
	$3d_{3/2}$	209.2	2.23	8.21	GL(30)	847	9.8
NbO_x	$3d_{5/2}$	204.4	2.23	8.21	GL(30)	3432	39.2
	$3d_{3/2}$	207.3	2.23	8.21	GL(30)	2265	25.9
Nb^0	$3d_{5/2}$	202.4	2.23	8.21	GL(30)	546	3.2
	$3d_{3/2}$	205.2	2.23	8.21	GL(30)	387	4.4

c) NbONP; 1s C analysis (before sputtering)

Peak Identity	Peak Type	BE (eV)	FWHM	R.S.F	Fit	Area	% Area
C-C	1s	284.4	1.29	1.00	GL(30)	7976	50.3
C-O	1s	285.5	2.16	1.00	GL(30)	7360	46.4
C=O	1s	288.3	1.27	1.00	GL(30)	523	3.3

d) Bulk, commercial $Nb_2O_5 \bullet H_2O$; Nb analysis (before sputtering)

Peak Identity	Peak Type	BE (eV)	FWHM	R.S.F	Fit	Area	% Area
Nb_2O_5	$3d_{5/2}$	206.7	1.02	8.21	GL(30)	16465	49.1
	$3d_{3/2}$	209.5	1.02	8.21	GL(30)	10867	32.4
NbO_x	$3d_{5/2}$	205.2	2.21	8.21	GL(30)	3744	11.2
	$3d_{3/2}$	208.0	2.21	8.21	GL(30)	2471	7.4

e) Bulk, commercial $Nb_2O_5 \bullet H_2O$; Nb analysis (after sputtering)

Peak Identity	Peak Type	BE (eV)	FWHM	R.S.F	Fit	Area	% Area
Nb_2O_5	$3d_{5/2}$	207.0	1.83	8.21	GL(30)	14459	28.9
	$3d_{3/2}$	209.8	1.83	8.21	GL(30)	9543	19.1
NbO_x	$3d_{5/2}$	204.2	2.96	8.21	GL(30)	16238	32.5
	$3d_{3/2}$	207.0	2.96	8.21	GL(30)	9791	19.6

3.5 References

1. Vo, V. H.; Khanh, B. T. H. L., *J Phys-Condens Mat.* **2009,** *21* (7).
2. Calo, V.; Nacci, A.; Monopoli, A.; Laera, S.; Cioffi, N., *J. Org. Chem* **2003,** *68* (7), 2929-2933.
3. Fan, X. L.; Xiao, X. Z.; Chen, L. X.; Wang, X. H.; Li, S. Q.; Ge, H. W.; Wang, Q. D., *J Mater Chem A* **2013,** *1* (37), 11368-11375.
4. Wang, H.; Ji, S.; Wang, W.; Wang, R. F., *S.A.J.C.* **2013,** *66*, 17-20.
5. Malyshev, D.; Bosca, F.; Crites, C. O.; Hallett-Tapley, G. L.; Netto-Ferreira, J. C.; Alarcon, E. I.; Scaiano, J. C., *Dalton transactions* **2013,** *42* (39), 14049-52.
6. Sattler, K. D., *Handbook of nanophysics*. CRC; London: Taylor & Francis., 2011.
7. Urban, J.; Sack-Kongehl, H.; Weiss, K., *Catal Lett* **1997,** *49* (1-2), 101-108.
8. Jha, M.; Ramanujachary, K. V.; Lofland, S. E.; Gupta, G.; Ganguli, A. K., *Dalton transactions* **2011,** *40* (31), 7879-7888.
9. Markowicz, A., *Pramana-J Phys* **2011,** *76* (2), 321-329.
10. Aufray, M.; Menuel, S.; Fort, Y.; Eschbach, J.; Rouxel, D.; Vincent, B., *J. Nanosci. Nanotechno.* **2009,** *9* (8), 4780-4785.
11. Grundner, M.; Halbritter, J., *J. Appl. Phys.* **1980,** *51* (1), 397-405.
12. Nowak, I.; Ziolek, M., *Chem. Rev.* **1999,** *99* (12), 3603-3624.
13. Maretti, L.; Billone, P. S.; Liu, Y.; Scaiano, J. C., *J.A.C.S.* **2009,** *131* (39), 13972-13980.
14. Pohlers, G.; Scaiano, J. C.; Sinta, R., *Chem. Mat.* **1997,** *9* (12), 3222-3230.
15. Feke, G. D.; Grober, R. D.; Pohlers, G.; Moore, K.; Cameron, J. F., *Anal. Chem.* **2001,** *73* (14), 3472-3480.
16. Tanabe, K.; Okazaki, S., *Appl Catal a-Gen* **1995,** *133* (2), 191-218.
17. Iizuka, T.; Ogasawara, K.; Tanabe, K., *B Chem. Soc. Jpn.* **1983,** *56* (10), 2927-2931.
18. Batamack, P.; Vincent, R.; Fraissard, J., *Catal. Today* **1996,** *28* (1-2), 31-39.
19. Batamack, P.; Vincent, R.; Fraissard, J., *Catal. Lett.* **1996,** *36* (1-2), 81-86.

4 • NbONP as Sustainable Catalyst
Scaling Up Synthesis

4.1 NbONP as a Powdered Catalyst

The main topics of the thesis has been the synthesis, investigation of the mechanism of reaction, and characterization of NbONP. The concentration of niobium precursor used for the synthesis of NbONP was kept at 10 μM of $Nb(acac)_5$. Based on this low concentration of the precursor, NbONP are expected to appear in fM concentration in the solution. Such concentration was high enough to test the Brønsted acid activity of NbONP with a dye C_6, but the low concentration of particles represents a serious limitation towards future studies, in particular, applications in catalysis.

In order to test the performance of NbONP as Brønsted acid catalyst in organic reactions, we need to obtain NbONP in larger amounts and preferably as a powder. Nanoparticles in the form of a powder are easier to manipulate. For example, after a reaction is completed, the powder can be separated by centrifugation, then washed and be re-used again in a new reaction. Such process is an attractive choice for synthesis at the industrial scale. Furthermore, generating NbONP as a powder allows a use of particles in a variety of solvents, thus, we can expand the range of organic reactions that can be utilized with these nanoparticles.

4.2 Scaling up – Reaction Apparatus

The first limitation for scaling up is a physical size of glassware that is being used. The reactions were performed inside 7 mm × 7 mm quartz cuvettes with the maximum volume of ~5 mL. Clearly, this is a limited volume for the desired amount of particles and larger-size cuvettes are needed to overcome this limitation. Using larger cuvettes will also require a different UVB irradiation setup, because the Luzchem photoreactor will not fit large-size glassware.

The larger container must be able to hold at least 100 mL of volume, be made of quartz (to allow UVB light transmission), and should connect to the Schlenk line to keep the reaction solution under the inert atmosphere. **Figure 4.1** (left) illustrates the design for this desired glassware set-up and we were able to obtain such cuvette of the suitable dimensions. The magnetic stir bar with the plate was added for mixing of the solution. Furthermore, as an alternative to the Luzchem photoreactor, it was decided to surround the reactor with the three UVB panels (each containing five UVB lamps, **Figure 4.1, right**) that together produced the same light intensity as in the small reactor used before.

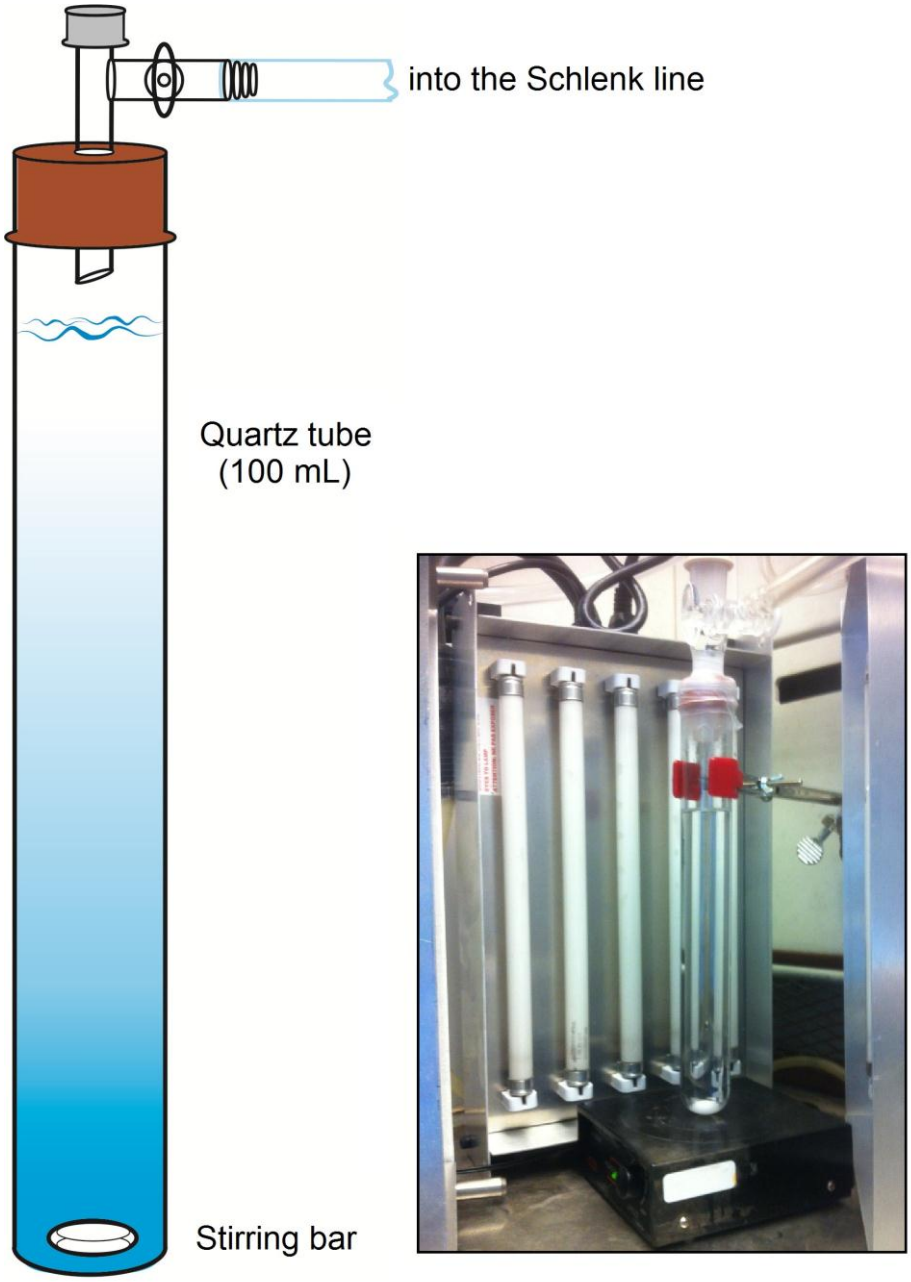

Figure 4.1 Graphical illustration of designed apparatus (left), where 100 mL of prepared solution is being kept under the inert atmosphere. Inset on the right is an actual picture of this set-up with the three UVB panels surrounding it (to the total of 15 UVB lamps).

This reactor was successfully tested in synthesis of NbONP from a solution of $Nb(acac)_5$ with I-907. The generated particles were isolated using centrifugation and dried as a powder. The composition of this powder was studied using XPS (as described in Chapter 3) and characterized with TEM (**Figure 4.2**, below) illustrating a formation of particles with 110 nm mean size.

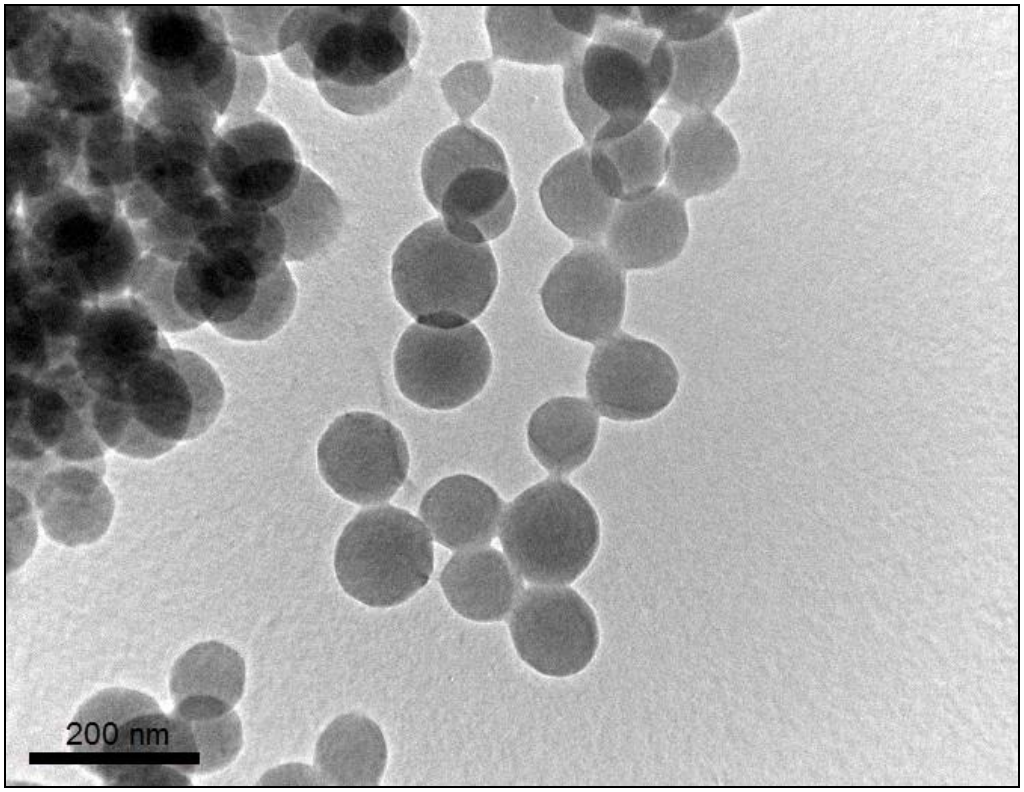

Figure 4.2 TEM image of NbONP powder prepared using the scaled up method from the solution of 420 µM Nb(acac)5 and 10 mM of I-907.

While this reactor has been designed and tested, it still needs further optimization (part for the future studies in the group). Optimization of this system can allow a production of NbONP in high yields to permit the evaluation of these particles as a catalyst in organic reactions. However, prior to any further optimizations, there are some limitations that have been found and are discussed below.

4.3 Limitations

The following is the description of problems that have been discovered. These issues need to be addressed:

i) After the irradiation of 100 mL solution containing 10 mM I-907, where the concentration of $Nb(acac)_5$ was higher than 450 μM, a formation of a white precipitate was observed (Nb_2O_5). As characterized with TEM, this precipitate is not NbONP.

ii) Increasing the concentration of I-907 above 10 mM provided no aid in preventing the formation of the white precipitate. In fact, this problem is independent to the concentration of I-907 that is being used.

Numerous attempts at trying to overcome the concentration limit of 450 μM $Nb(acac)_5$ have been made. This issue has also been previously displayed before with the small scale reactions. The same precipitate is formed when the concentration higher than 10 μM $Nb(acac)_5$ were used in 7 mm x 7mm quartz cuvettes, hence all of the small scaled reactions were set at that limit.

There seems to be a strong relationship between the concentration of $Nb(acac)_5$ used and the successful generation of NbONP. In this dependable relationship an increased amount of volume must be made when the higher concentration of $Nb(acac)_5$ are sought after. This scaling up work is in need of further investigation, possibly either moving it up into the higher-volume solutions or simply searching for additional stabilizers for the additional control during the reaction.

4.4 Experimental Details

General

The preparation of stock solution of 208 mM $Nb(acac)_5$ was described in details in Chapter 2. This stock solution was previously used for small scale reactions and is used here for the scaling up synthesis. HPLC grade acetonitrile was purchased from Sigma Aldrich and purified using a LC Technology Solvent Purification System fitted with an alumina column. All glassware was thoroughly cleaned, rinsed with Millipore water and dried at 130°C prior to use. Hot glassware was immediately sealed and purged with Industrial T (99.9%) argon gas after removal from the oven.

NbONP Scale up Sample Preparation

10 mM solution of I-907 was prepared by loading 280 mg of I-907 with 100 mL of CH_3CN inside the dry 250 mL round bottom flask. This solution was shaken thoroughly, kept under inert atmoshere and received an addition of 150 μL of 280 mM $Nb(acac)_5$ stock solution (to a final concentration of 420 μM $Nb(acac)_5$). The reaction mixture was then shaken thoroughly and transferred via a double-ended needle into the sealed 100 mL large quartz cuvette (shown in **Figure 4.1**) and irradiated for 480 min at r.t. surrounded by three Luzchem panels equipped with 15 UVB bulbs (λ=281-315 nm; 71 W/m^2). The solution was stirred during reaction to allow a homogeneous irradiation.

After the irradiation, the solution changed its color from transparent clear into yellow. The solution was then exposed to air and separated into 15 mL centrifugation tubes (by 10 mL for a total of 10 tubes). After being stored overnight inside the standard refrigerator, the solution in these tubes was centrifuged for 30 min at 10000 rpm. After the centrifugation a supernatant was removed leaving a white precipitate that was re-suspended in 5 mL of clean acetonitrile and then centrifuged again for 30 min at 10000 rpm. The resulting powder was studied using XPS (as described in Chapter 3) and with TEM (**Figure 4.2**). The TEM measurements confirm the formation of the particles with a 110 nm mean size.

5 • Conclusion:
Future Directions

5.1 Summary

In this work, we developed a method to the photochemical synthesis of NbONP. The mechanistic study of formation of particles was investigated first (Chapter 2), followed by particles property characterization (Chapter 3). By studying the mechanism of formation we learned how to control the size of NbONP, without which we would not be able to obtain a library of nanoparticles with different sizes.

The initial investigation of mechanism demonstrated that, when the reaction solution with increased concentration of I-907 was irradiated, higher concentrations of I-907 side products were produced. These side products are capable of acting as mild reducing agents that support continuous growth of NbNP over 300 minutes of irradiation. Therefore, we obtained the data for the size of NbONP generated when the specific concentration of I-907 are used. Using these data as a guide, particles with the specific size can be selectively generated.

Furthermore, the studies of I-907 mechanism allowed to identify the photogenerated mild reducing agent as MSBA. The control experiments with MSBA confirmed that this chemical is indeed responsible for the growth of NbONP. Consequently, we tested MSBA with $Nb(acac)_5$ directly for the synthesis of NbONP. Such experiment was very successful and we were able to reproduce the previously established I-907 trend of the particles size increase, but this time substituting I-907 with MSBA as the only reducing agent.

To gain further insights into the mechanism of particles formation with MSBA, the GC-MS analysis of irradiated MSBA was performed. The results of GC-MS illustrated that MSBA, upon photoexcitation, is excited into the triplet state ^{3}MSBA. Then, an outer-sphere electron

transfer from ^{3}MSBA to Nb^{5+} takes place. This reduction of the niobium ions forms the seeds, which can then grow into the larger NbNP.

Exposure of NbNP to oxygen causes their oxidation leading to the formation of NbONP. In order to characterize this process, NbONP were investigated using a variety of techniques (XPS, EDS and HRTEM; Chapter 3) that demonstrated the core-shell structure of the nanoparticles. These methods indicated that the core is metallic Nb^0 and the shell is the niobium oxide, Nb_2O_5.

Since Nb_2O_5 is a strong Brønsted acid, we tested the Brønsted activity of NbONP with pH sensitive dye coumarin-6 (C_6) (monitored using fluorescence and UV-vis, Chapter 3). The results of these spectroscopic experiments indicated that NbONP can protonate C_6, thus serving as confirmation for the acidity of NbONP. Furthermore, particles with varying sizes were tested with C_6 to check if the difference in size affects the acidity. It was observed that the particles with the larger sizes have the strongest acidity and the particles of smaller sizes (mean size less than 60 nm) are less acidic and cannot protonate C_6 effectively.

On the whole, the photochemical synthesis of NbONP is a novel approach in which no strongly reducing agents are needed and particles with a reproducible size are formed. The methodology in this study is an example of how nanoparticles can be developed using principles of both photo- and organic chemistry, with the strong backup of the surface characterization techniques.

5.2 Future Studies

While this work shows the completed investigation into the formation and characterization of NbONP, there are few areas that are still open for future studies. Specifically, there are two directions which will be worth exploring: i) the structural investigation of $Nb(acac)_5$, and ii) the optimization of conditions for a scaled-up NbONP synthesis.

In Chapter 4, a successful method for the scaled-up synthesis of NbONP using 100 mL quartz tube has been described. However, this approach has limitations (listed in section 4.3 of Chapter 4) and can be the subject to further optimization.

As mentioned, the major challenge is to move away from the use of low precursor concentrations. After the synthesis of NbONP is optimized for a higher yield production, the nanoparticles can be then isolated as a powder. This will be essential in exploring catalytic applications of NbONP for a various reactions.

5.3 Publications Resulting from Work Presented in this Thesis

Malyshev, D., Bosca, F., Crites, C. O., Hallett-Tapley, G. L., Netto-Ferreira, J. C., Alarcon, E. I., and Scaiano, J. C. "Size-controlled photochemical synthesis of niobium nanoparticles", *Dalton Transactions*, **2013**, 42 (39), 14049-52.